Tayyibe BARDAKÇI

STRUCTURAL AND SPECTROSCOPIC INVESTIGATION OF SOME COPPER(II) COMPOUNDS

by

Tayyibe BARDAKÇI

M.S. Thesis In Physics

June - 2010

June 2010

STRUCTURAL AND SPECTROSCOPIC INVESTIGATION OF SOME COPPER(II) COMPOUNDS

by

Tayyibe Bardakçı

A thesis submitted to

The Graduate Institute of Sciences and Engineering

of

Fatih University

in partial fulfillment of the requirements for the degree of

Master of Science

in

Physics

June 2010
Istanbul, Turkey

APPROVAL PAGE

I certify that this thesis satisfies all the requirements as a thesis for the degree of Master of Science.

Prof. Dr. Mustafa KUMRU
Head of Department

This is to certify that I have read this thesis and that in my opinion it is fully adequate, in scope and quality, as a thesis for the degree of Master of Science.

Prof. Dr. Mustafa KUMRU
Supervisor

Examining Committee Members

Prof. Dr. Mustafa KUMRU _____

Prof. Dr. Ayhan BOZKURT _____

Assist. Prof. Kurtuluş GÖLCÜK _____

It is approved that this thesis has been written in compliance with the formatting rules laid down by the Graduate Institute of Sciences and Engineering.

Assoc. Prof. Nurullah ARSLAN
Director

Date
June 2010

STRUCTURAL AND SPECTROSCOPIC INVESTIGATION OF SOME COPPER(II) COMPOUNDS

Tayyibe BARDAKÇI

M. S. Thesis – Physics
June 2010

Supervisor: Prof. Dr. Mustafa KUMRU

ABSTRACT

In this study, transition metal complexes, $Cu[p\text{-}tol]_2Cl_2$ and $Cu[m\text{-}tol]_2Cl_2$ are synthesized. In order to determine and investigate these complexes, elemental analysis, infrared and Raman spectroscopy techniques are used. In these complexes p-tolouidine and m-tolouidine have been used as ligands and the geometrical structure and vibrational frequencies of ligands have been obtained by using Density Functional Theory (DFT). DFT-B3LYP, DFT-B3PW91, and DFT-PBEPBE methods with 6-311G+** and aug-ccPVQZ basis sets have been used in calculations. The experimental infrared and Raman vibrational modes of ligands have been determined by DFT calculation results. These characteristic ligand bands have been observed in the infrared and Raman spectra of the complexes. However, some shifts have also been observed in some ligand bands. These shifts represent metal chloride's forming bonds with ligands, p-tolouidine and m-tolouidine.

Keywords: Infrared and Raman Spectroscopy, Density Functional Theory (DFT), transition metal complex, p-tolouidine, m-tolouidine.

BAZI BAKIR BİLEŞİKLERİNİN YAPISAL VE SPEKTROSKOPİK İNCELENMESİ

Tayyibe Bardakçı

Yüksek Lisans Tezi – Fizik
Haziran 2010

Tez Danışmanı: Prof. Dr. Mustafa KUMRU

ÖZ

Bu çalışmada geçiş metal kompleksleri $Cu[p\text{-}tol]_2Cl_2$ ve $Cu[m\text{-}tol]_2Cl_2$ sentezlenmiştir. Kompleksleri tanımlamak ve incelemek için elemental analiz, infrared ve Raman spektroskopi teknikleri kullanılmıştır. p-tolouidine ve m-tolouidine bu komplekslerde ligand olarak kullanılmıştır ve bu ligandların geometrik yapıları ve titreşim frekansları Yoğunluk Fonksiyonel Teori (DFT) kullanılarak elde edilmiştir. Hesaplamalarda DFT-B3LYP, DFT-B3PW91 ve DFT-PBEPBE metotları 6-311G+** ve aug-ccPVQZ temel kümeleri ile birlikte kullanılmıştır. Ligandların deneysel infrared ve Raman modları DFT sonuçları ile elde edilmiştir. Komplekslerin infrared ve Raman spektrumlarında karakteristik ligand bantları gözlemlenmiştir. Bazı bantlarda kaymalar gözlemlenmesi, metal klorürün p-tolouidine ve m-tolouidine ile bağ yaptığını göstermiştir.

Anahtar Kelimeler: Infrared ve Raman Spektroskopi, Yoğunluk Fonksiyonel Teori (DFT), gecis metal kompleksi, p-tolouidine, m-tolouidine.

ACKNOWLEDGEMENT

I express sincere appreciation to Prof. Dr. Mustafa Kumru for his guidance and insight throughout the research.

Thanks go to the other faculty members, Assist. Prof. Kurtuluş Gölcük and Assist. Prof. Levent Sarı, for their valuable suggestions and comments, and always helping me in problems. The technical assistance of İbrahim Şaşmaz, İsmail Anıl, and Sevim Üngür Çelik are gratefully acknowledged.

I also want to thank all members of Physics Department, especially to my roommate Dr. Vesile Güçlü and my colleague and my friend Hüseyin Kavas, and Ali Karatutlu always willing to help and share the problems.

I am thankful to all my friends for their motivation and support especially Aslıhan Cesur, Aslı Demiryas, Eda Baykal Çağlar, Gizem Berber, Halid S. Şimşek, Mehmet Çakır, Neslihan Parlar, Özgür Aydoğan, Tuğba Çelik and Zeynep Arkan.

Lastly, but in no sense the least, I express my thanks and appreciation to my family for their understanding, motivation and continuous support throughout my life.

TABLE OF CONTENTS

LIST OF TABLES

LIST OF FIGURES

LIST OF SYSMBOLS AND ABBREVIATIONS

SYMBOL/ABBREVIATION

DFT : Density Functional Theory

HF : Hartree-Fock

$n(r)$: Electron density

$v(r)$: External potential

TF : Thomas-Fermi

E_{XC} : Exchange correlation energy

LDA : Local Density Approximation

GGA : Generalized Gradient Approximation

WDA : Weighted Density Approximation

B3LYP : Becke's three-parameter in combination with the Lee-Yang-Parr

PW91 : Perdew and Wang's 1991 gradient-corrected correlation functional

PBE : The 1996 gradient-corrected correlation functional of Perdew, Burke and Ernzerhof

B95 : Becke's τ-dependent gradient-corrected correlation functional

VWN : Vosko, Wilk, and Nusair 1980 correlation functional

ν : Frequency

ATR : Attenuated total reflectance

IR : Infrared

FT : Fourier transform

μ : Induced electric dipole

α : Polarizability

β : The rate of polarizability

Å : Angstrom

a.u : Atomic unit

CHAPTER 1

INTRODUCTION

Aniline is an organic compound having the formula C_6H_7N also known as phenylamine, aminobenzene or benzamine. Aniline and its substituted derivatives have great commercial value, especially in dyestuffs. In addition to its use in dyestuffs, it has been widely used as starting materials in the formation of many drugs (i.e. paracetamol), rubber processing chemicals, pesticides, antitoxidans, electro-optical and many other industrial processes [1-14].

When polymerised, aniline can be used as a type of nanowire in microelectric devices, or some of the para-substituted derivatives of aniline can be used as local anesthetics, and the amino group in these molecules plays an important role in the interaction with receptor. Hence, theoretical and experimental studies about their structure, molecular properties or their reaction mechanisms have great importance [15-19].

When aniline derivatives are prepared from nitrated aromatic compounds, we can reach toluidines. Tolouidines are organic compounds, and have three isomers which are p-tolouidine, m-tolouidine, and o-tolouidine. The p- refers para, the m- refers meta, and the o-refers ortho. These three isomers have similar structure with aniline, but a methyl group is substituted to the aromatic ring. In this study, p-tolouidine and m-tolouidine will be examined structurally and spectroscopically. The difference between these two isomers is the position of methyl group (CH_3) relative to the amino group (NH_2).

In p-tolouidine (4-C_7H_9N or 4-(CH_3)-$C_6H_4NH_2$) a methyl group is attached at the para position of aniline and it is also known as p-methylaniline, 4-methylaniline, p-aminotoluene, 4-aminotouluene, or 1-amino-4methylbenzene.

Figure 1.1 The molecular structure of p-tolouidine

Wheras in m-toluidine (3-C_7H_9N or 3-(CH_3)-$C_6H_4NH_2$) a methyl group is attached at the meta position of aniline and it is also known as m-methylaniline, 3-methylaniline, m-aminotoluene, 3-aminotoluene, or 1-amino-3methylbenzene.

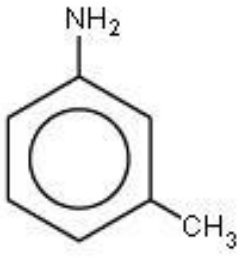

Figure 1.2 The molecular structure of m-tolouidine

Transition metal complexes of aniline and its derivatives generally have the formula ML_2X_2. In that formula M is metal, L is ligand and X is the halogen such as Cl, Br or I.

In literature, vibrational analysis of transition metal complexes with p-tolouidine and m-tolouidine have been studied in various works. Golcuk et al., in 2003a has studied thermogravimetric (TG) behaviors and vibrational analyses of [Zn(II), Cd(II), and Hg(II)] bromide complexes with m-tolouidine [20].

Altun et al., in 2003a has reported FT-IR and FT-Raman spectroscopic study of [Ni(II), Zn(II), and Cd(II)] iodine complexes with m-tolouidine complexes [21].

Altun et al., in 2003b, has examined thermal behaviours and vibrational (including both FT-IR and FT-Raman) spectra of [Zn(II), Cd(II), and Ni(II)] iodine complexes with p-tolouidine complexes [22].

Golcuk et al., in 2003b has investigated thermogravimetric (TG) behaviors, magnetic moments, electronic spectra and vibrational spectra of the metal(II) [Mn(II), Co(II), and Ni(II)] bromide with m-tolouidine complexes [23].

Golcuk et al., in 2004 has reported thermogravimetric (TG) behaviors, vibrational and EPR spectral studies of copper(II) bromide complexes with p-tolouidine and m-tolouidine [24].

Golcuk et al. in 2005, has reported thermal analysis and FT-IR and FT-Raman spectroscopic studies of metal(II) [Zn(II), Cd(II), and Hg(II)] bromide complexes with p-tolouidine complexes [25].

In this study, transition metal Cu^{+2} complexes of p-tolouidine and m-tolouidine compounds with chlorine, Cu $[p\text{-tol}]_2$ Cl_2 and Cu $[m\text{-tol}]_2$ Cl_2 are synthesized and investigated, see Figure 1.3. In order to determine these complexes, elemental analysis, FT-Infrared and the dispersive Raman spectroscopy techniques are used. In literature, in a variety of works, the applicability of traditional and Density Functional Theory (DFT) methods to the experimental data on anilines (which are used as ligands in these complexes) have been discussed.

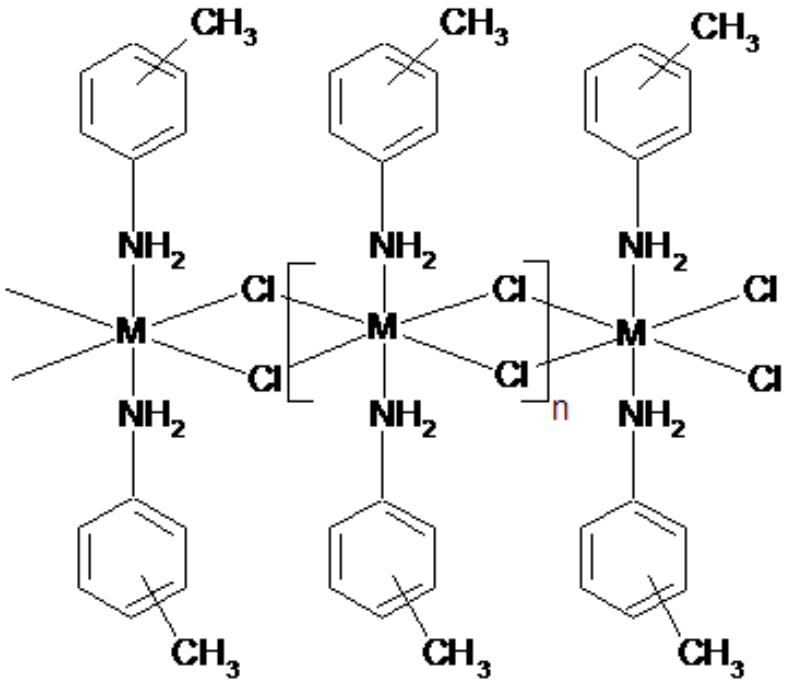

Figure 1.3 Transition metal Cu^{+2} complexes of p-tolouidine and m-tolouidine compounds with chlorine.

Altun etl al., in 2003c have examined the theoretical and experimental studies of the vibrational spectra of m-tolouidine [26]. Altun etl al., in 2003 has also examined structure and vibrational spectra of p-tolouidine by using Hartree-Fock, MP2 and DFT calculations [27].

Kurt et al., in 2004 have reported the molecular structure and vibrational frequencies of 3-chloro-4-methyl aniline in the ground state by DFT and ab initio Hartree-Fock calculations [28].

Krishnakumar and Balachandran in 2005 have studied the vibrational spectra and DFT calculations of the 2,6-dibromo-4-nitroaniline and 2-(methylthio)aniline [29].

Krishnakumar and Muthunatesan in 2005 have examined the DFT and FT-IR and FT-Raman spectra of 4-chloro-5-fluoro-1,2-phenylenediamine ($C_6H_6ClFN_2$) [30].

Sundaraganesan et al., in 2005 have reported the FT-IR, FT-Raman spectra and ab inito DFT vibrational analysis of 2-bromo-4-methyl-phenylamine [31].

El-Gogary, T.M., et al., in 2006 have studied spectroscopic and quantum mechanical studies of substituted anilines and their charge-tansfer complexes with iodine in different solvents [32].

Rai et al., in 2006 have studied the infrared and Raman spectra of chlorine substituted anilines. Vibrational frequencies of these molecules have been calculated with DFT and Hartree-Fock methods [33].

Arjunan and Mohan in 2008 have examined the Fourier transform infrared (FT-IR) and FT-Raman spectral analysis of 4-chloro-3-methylaniline. The vibrational frequency are compared with theoretical results obtained from Hartre-Fock and DFT calculations [2].

In 2009, Arjunan and Mohan have also examined the Fourier transform infrared (FT-IR) and FT-Raman spectral analysis of 2-chloro-4-methylaniline and 2-chloro-6-methylaniline. The vibrational frequency are compared with theoretical results and the geometries and normal modes of vibration obtained from Hartre-Fock and DFT calculations [34].

Within all these studies DFT calculations have been found very promising for vibrational spectra analyses. Thus, the geometrical structure and vibrational frequencies of ligands, p-tolouidine and m-tolouidine, are calculated with Density Functional Theory (DFT). In DFT calculations B3LYP, B3PW91 and PBEPBE methods are used with 6-31G+** and aug-ccPVQZ basis sets.

CHAPTER 2

THEORETICAL APPROACH

2.1 Density Functional Theory

Density Functional Theory (DFT), used in physics to investigate the electronic structure of many body systems, in particular atoms, molecules, and the condensed phases, is one of the most successful and widely-used quantum mechanical approaches to matter [35-37]. DFT is applied in calculation of vibrational frequencies, geometric parameters, and binding energy of molecules. Besides, atoms in the focus of strong laser pulses, classical liquids, super conductivity can be studied with DFT. In addition to its usage in physics it is widely used in other disciplines, such as quantum chemistry, biology, and mineralogy, etc. [35, 38-39].

DFT has been very popular for calculations in molecular physics when compared with traditional ways, such as Hartree-Fock Theory and its descendants. Since, the results of calculations in DFT compatible with the experimental data, and computational costs were relatively low, DFT calculations are preferable. On the other hand, in the case of few atomic systems, such as number of atoms are near to 5-10, and when high accuracy is required Hartree-Fock may be more suitable [40].

In DFT, the most notable thing is the expressing electronic ground state energy in terms of electron density $n\,(r)$[37, 38-42]. This method was first introduced by P. Hohenberg and W. Kohn in 1964, and they suggested that the density may be used in place of the external potential.

$$n\,(r) \rightarrow v(r) \qquad 2.1$$

For a given external potential $v(r)$, energy can be expressed as a functional of the electron density;

$$E[n(r)] = \int v(r)\, n\,(r) dr + F[n(r)] \qquad 2.2$$

here,

$$F[n(r)] = (\psi[n(r)], (T + U)\psi[n(r)]) \qquad 2.3$$

where $\psi[n(r)]$ is the N-particle ground state wave function.

If some approximations are applied to $F[n(r)]$, it can be easily reached to Thomas-Fermi approximation [40]. It is one of the simplest models of the electronic structure of atoms was derived by Thomas and Fermi in 1927. In order to approximate the distribution of electrons in an atom they preffered a statistical model.

$$T_{TF}[n(r)] = C_F \int n(r) n^{\frac{2}{3}} r\, d^3 r = C_F \int n^{\frac{5}{3}} r\, d^3 r \qquad 2.4$$

where $C_F n^{\frac{5}{3}}(r)$ is the kinetic energy density of a uniform electron density $n\,(r)$. Besides this, just using electrostatic term only, Thomas and Fermi approximated the Coulomb interaction energy of the electrons.

In Thomas Fermi Model, $E_{XC}[n(r)]$ is taken 0.

However,

$$F[n(r)] = T_s[n\,(r)] + \frac{1}{2} \int \frac{n(r)\, n(r')}{|r - r'|} dr\, dr' + E_{XC}[n(r)] \qquad 2.5$$

In the equation, $T_s[n\,(r)]$ is the kinetic energy of the non-interacting electrons, and the second term is the classical expression for the interaction energy. Then, $E_{XC}[n(r)]$ is the exchange correlation energy, that includes the remaining part of the electron-electron interactions.

Ignoring exchange correlation energy, will take us Kohn-Sham equations. In Kohn-Sham equations a reference system of independent non-interacting electrons has

the same density as the real fully interacting system is considered [42-43]. That is a set of independent reference orbitals φ_i satisfies the independent particle Schrödinger equation:

$$\left(-\frac{1}{2}\nabla^2 + v(r) + \int \frac{n(r')}{|r-r'|}\,dr' + v_{xc}(r) - \in_i\right)\varphi_i(r) = 0 \qquad 2.6$$

$$n(r) = \sum_{j=1}^{N} |\varphi_i(r)|^2 \qquad 2.7$$

$$v_{xc}(r) = \frac{\delta E_{XC}[n(r)]}{\delta n(r)} \qquad 2.8$$

The only difference between Kohn-Sham euqations and Hartree equations is the inclusion of exchange correlation potential by Kohn-Sham equations. As in the Hartree equations, local equations shoul be solved in a self-consistent way, and exchange correlation potential v_{xc} should be calculated in each cycle by choosing suitable approximation for exchange correlation energy E_{XC}. Thus it can be said that, if it is an error in the theory, it is because of the approximations of $E_{XC}[n(r)]$.

In Kohn-Sham equations the ground state energy is given by:

$$E = \sum_1^v \in_i - \frac{1}{2}\int \frac{n(r)\,n(r')}{|r-r'|}dr\,dr' - \int v_{xc}(r)\,n(r)dr + E_{XC}[n(r)] \qquad 2.9$$

Hence, in order to evaluate the $E_{XC}[n(r)]$, some approximations are made. One of the most widely used approximation in phycics is the local density approximation (LDA) [27]. Although it is the simplest one, it is very usable, since the functional depends only on the density at the coordinate where the functional is evaluated.

$$E_{XC}^{LDA}[n(r)] = \int \in_{XC}\left(n(r)\right)n(r)dr \qquad 2.10$$

where $\in_{XC}$ is the exchange correlation energy per particle of a uniform interacting electron gas with a density $n(r)$. It means that, electrons uniformly spread out in a cube and with the uniform distribution of the positive charge, system will be neutral. That is, charge density changes slowly in the molecule, and thus a localized region of the molecule behaves like a uniform electron gas.

Beyond LDA, there are also density fuctionals such as generalized gradient approximation (GGA) and the weighted density approximation (WDA). Different from LDA, GGA is still local, but it also takes into account the gradient of the density at the same coordinate. On the other hand, WDA offers an example of genuinely nonlocal functional.

In DFT calculations, in order to determine the properties of many-electron system, functionals are used and how they deal with exchange correlation energy is remarkable. As it mentioned above, for a general inhomegeneous system LDA approximates the exchange correlation energy density. On the other hand, there are Hybrid functionals, which are a class of approximations to the exchange correlation energy functional in DFT, include exact term in the exchange functional, differently from traditional functionals. In the formation of a Hybrid functional, one shoul be empiric, while choosing the functionals mixed in the Hartree-Fock and DFT terms [26]. For instance, one of the most common and successful Hybrid function is B3LYP (Becke's three-parameter in combination with the Lee-Yang-Parr). In B3LYP, Becke's exchange functional, is combined with the exact energy from Hartree-Fock theory. Here, B3 specifies how much of the exact exchange is mixed in; 20% HF, 8% Slater, and 72% is the Becke-88 [42-45]. However, LYP includes both local and non-local terms:

$$E_{XC} = a\,E_X^{Slater} + (1-a)E_X^{HF} + b\Delta E_X^{Becke-88} + E_C^{VWN} + c\Delta E_C^{non-local} \qquad 2.11$$

where a,b, and c are the constants determined by Becke and VWN is used to provide the excess local correlation required, since LYP contains a local term essentially equivalent to VWN.

Differently from B3LYP, there are also many exchange and correlation functionals and in order to produce a usable method they must be combined with each other. Some of them used in Gaussian software package are, PW91 (Perdew and Wang's 1991 gradient-corrected correlation functional), PBE (The 1996 gradient-corrected correlation functional of Perdew, Burke and Ernzerhof), B95 (Becke's τ-dependent gradient-corrected correlation functional (defined as part of his one parameter hybrid functional), VWN (Vosko, Wilk, and Nusair 1980 correlation functional) [45].

2.1.1 Basis Set

A basis set is a serie of basis functions, which is used in showing molecular orbitals. These molecular orbitals are a linear combination of basis functions with the various coefficients. Although basis sets are examined in two categories; Slater Type Orbitals, and Gaussian Type Orbitals, the latter is preferable because of the easy calculation of integrals in Gaussian basis functions, so this brings computational efficiency.

Gaussian Type Orbitals inlude a wide range of basis sets and most common of these are, minimal basis sets, Pople type split-valence basis sets, polarized basis sets, and correlation consistent basis sets. Minimal basis sets are the smallest of these, since they are composed of the minimum number of basis functions required to show the electrons on each atom. Pople type split-valence basis sets are the most widely used ones and they cause the change in size instead of shape in orbitals. 3-21G, 6-31G, and 6-311G are the commonly used of this type. Polarized basis sets occur as a result of addition of polarization functions, which is denoted by an asterisk, *, or (d). It means polarization basis set is used where d functions are added to heavy atoms. Two asteriks, **, or (d,p) indicate that polarization functions are also added to light atoms. And the last one, correlation consistent basis sets occur as a result of addition of diffuse functions, which is denoted in Pople type split-valenced sets by a plus sign, +, and in Dunning type sets by augmented, aug. And as in the case of polarization functions two plus sign means, diffuse functions are also added to light atoms [46-48].

2.2 Vibrational Spectroscopy

""... everything that living things do can be understood in terms of the jigglings and wigglings of atoms."" Richard P. Feynman [49]

A molecule with N atoms can move continuously as in the forms of rotation, translation and vibration. The position of these N atoms can be determined with 3N coordinates, so it can be said that this molecule has 3N degrees of freedom and each degree of freedom is used to perform an independent movement [50-52].

A non-linear molecule with N atoms has 3N-6 vibrational degrees of freedom. Since the rotational movement uses three degrees of freedom, and also the translational movement uses three degrees of freedom of total 3N degrees of freedom, only internal vibrations are allowed.

Moreover, a linear molecule with N atoms has 3N-5 vibrational degrees of freedom. Because, in linear molecules there is no rotational movement around the bond axis.

A molecule with N atoms has N-1 strecting motions of bonds, since it has N-1 bonds between these N atoms. Therefore, remaining 2N-5 are bending motions for non-linear molecules and 2N-4 for linear molecules.

2.2.1 Infrared Spectroscopy

Infrared spectroscopy gives detailed information about the structure of molecules by the way of the frequencies of the normal modes of vibrations, and deals with the absorption of light in the infrared region of the electromagnetic spectrum.

In infrared spectrum in order to be infrared active there must be a nonzero dipole moment change during the vibration. For example if we consider HCl, H is relatively positive and Cl is relatively negative, and this molecule will act as a dipole. Thus, this molecular dipole moment oscillates about its equilibrum position too, and behaves as a simple harmonic oscillator. According to this simple harmonic model, oscillating dipole

absorbs energy only if the frequency of the incident light and the vibrations are the same.

In infrared spectrum light of all frequencies is passed through a sample, that is energy is transferred, and so a transition occurs between two energy levels. Since this light has frequency ν, the difference between the two vibrational energy levels is directly proportional to this frequency.

$$\Delta E = E_2 - E_1 = h\nu \qquad 2.12$$

One of the most important and allowed transitions which give strong absorption bands in the infrared are fundamentals. In fundamentals, transitions occur from the ground state ($\nu_i = 0$) to the first excited state ($\nu_i = 1$). In overtones, transitions occur from the ground state ($\nu_i = 0$) to the ($\nu_i = 2$) energy state. Besides these, in combinations transitions occur between two different vibrations ($\nu_i = 1$ to the $\nu_j = 1$ state). On the other hand, in infrared spectrum overtones and combinations correspond to weak absorptions due to the forbidding of simple harmonic oscillator theory of molecular vibrations.

In infrared spectroscopy, solid, liquid, and gas samples can be studied. Since the particles reflect and scatter the incident beam, generally transmittance is low in solids, thus they are more difficult to examine. If the dissolving of the solid is impossible, grinding it in nujol (paraffin oil) is a way, because of forming a suspension. Then this suspension can be held between salt plates. Besides this, grinding solids in potassium bromide is another technique. By applying very high pressure, and pressing the mixture into a transparent disk, sample may be placed directly in the infrared beam.

On the other hand, nowadays attenuated total reflectance (ATR) spectroscopy is widely used. ATR is a sampling technique, which enables sample to be examined directly whether it is solid, liquid, or gas state, without any preparation.

In ATR, a beam of infrared light is passed through the ATR crystal, and it reflects to the internal surface which is in contact with the sample. Then, the beam is collected by a detector. By mounting ATR apparatus to the infrared spectrometer's sample

compartment, spectra can be taken easily. Although it costs very high, because of its excellent mechanical properties generally diamond is preferable for ATR crystal.

2.2.1.1 Infrared Spectrometers

Starting from at the end of the 1940s infrared spectrometers have been using very common in order to take infrared spectra of molecules. Collecting data of infrared spectra of molecules for years, helps determination of the structure of molecules.

Nowadays, normal infrared can be taken between 4000 – 400 cm^{-1}, nevertheless in some infrared spectrometer this range can go to the far infrared, that is to 200 cm^{-1}.

Infrared spectra can be obtained by either dispersive or Fourier Transform methods.

Dispersive IR spectrometer includes three essential parts;

a) Source
b) monochromator
c) detector

Source in the dispersive IR spectrum has usually high resistance and provides continuous infrared radiation. Monochromator includes a grating part and it disperses radiation into its spectrum part, and a mechanical tool scans with different frequencies continuously, then a sensitive detector detects which frequencies have been absorbed or not by the sample.

On the other hand, instrument manufacturers do not prefer to manufacture dispersive IR spectrometers. However it plays an important role in the development of infrared spectroscopy and it still in use in some places.

Besides this, Fourier Transform Spectroscopy technique is also important for applying instantaneous and simultaneous recording of the spectrum in the infra-red region. And in FT method recording spectra is much more rapid compared with the conventional frequency sweep technique. Since the Fourier transform essentially

reduces the time spent obtaining a spectrum, the range of materials which can be studied in this technique is quite high.

Fourier transform infrared (FT-IR) spectrometer is based on Michelson interferometer. As in the Figure 2.1, the instrument has two plane mirrors, which are perpendicular to each other. One of the mirrors M_1 is fixed and the other one M_2 can move, which introduces a time delay. Light from the source splits 50% of the incident radiation to one mirror, and reflects 50% to the other. The radiation interferes, and allows the of the light to be measured at each different time delay setting. That converts time domain into a spatial coordinate. If the measurements are taken at many discrete positions of the movable mirror, the spectrum can be reconstructed using a Fourier transformof the temporary coherence of the light.

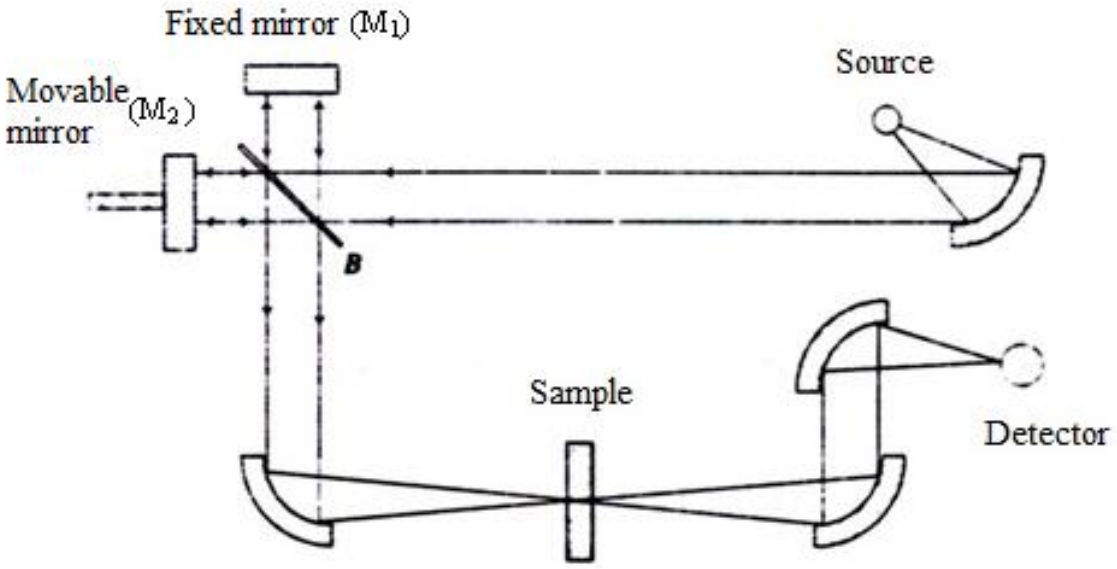

Figure 2.1 The Schematic illustration of the FT-IR Spectrometer [51]

2.2.2 Raman Spectroscopy

As in the case of infrared spectroscopy, Raman spectroscopy is a technique for identification and analysis of molecular structure. Raman spectrum is obtained by the result of the scattering of light. When a monochromatic radiation is applied from a laser,

the scattered energy will have the definite discrete frequencies above and below the incident monochromatic radiation. This process is called as Raman scattering.

In Raman scattering process there is an inelastic collision between photons and molecules, it means energy is exchanged; that is photons or molecules gain or lose energy. For instance, if ΔE is the energy change of the molecule, when molecule gains this energy, the scattered photon will have the energy $h\nu - \Delta E$, or when molecule loses energy, the photon will have the energy $h\nu + \Delta E$, vice versa.

As shown in the Figure 2.2 when incident radiation has higher energy than the scattered radiation, it is called as Stoke's scattering. However, when incident radiation has lower energy than the scattered, this time it is called as anti-Stoke's scattering. On the other hand, if it were elastic collision, there will be no energy exchange, so scattered radiation will be equal to the incident radiation's energy, which is referred to as Rayleigh scattering.

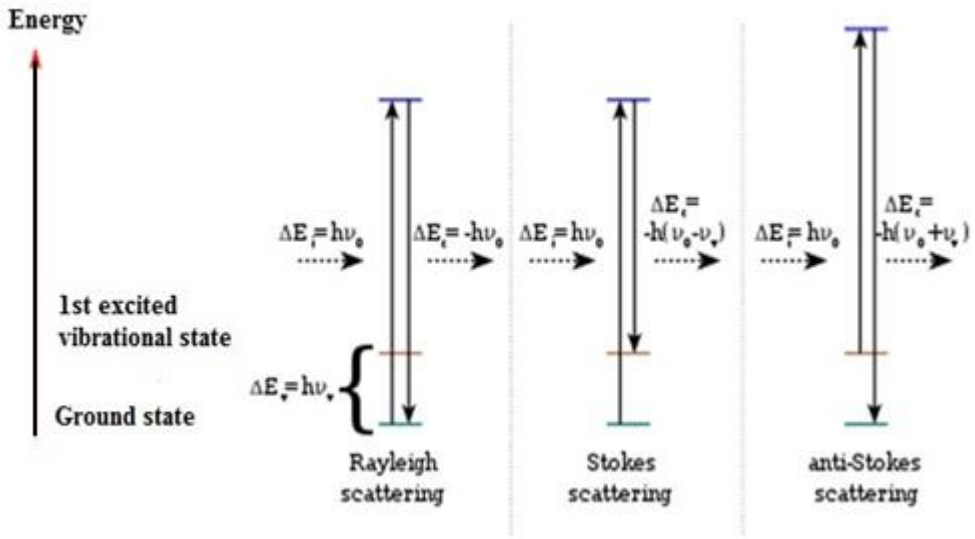

Figure 2.2 Raman Scattering [53]

In Raman spectrum, in order to be Raman active, rotation or vibration of molecules must make some difference in the polarizability of the molecule. If a molecule is placed in a static electric field, positively charged nuclei goes to the

negative pole of the field and negatively charged electrons go to the positive pole of the field. So there will be a separation between nuclei and electrons, and in order to keep them in the molecule, induced electric dipole forms. Thus this molecule can be said that as polarized, and it can be shown as

$$\mu = \alpha E \tag{2.13}$$

Here μ is the induced electric dipole, E is the applied electric field, and α is the polarizability of the molecule.

In the case of applying radiation with a frequency ν to these molecules, electric field can be shown as;

$$E = E_0 \sin 2\pi\nu t \tag{2.14}$$

hence, induced dipole oscillates because of this oscillating electric field, then;

$$\mu = \alpha E_0 \sin 2\pi\nu t \tag{2.15}$$

In addition to this oscillating dipole, molecules also start to make internal motions beacuse of vibrations. This changes the polarizability of the molecule as;

$$\alpha = \alpha_0 + \beta \sin 2\pi \nu_{vib} t \tag{2.16}$$

where α_0 is the equilibrium polarizability, and β is the rate of polarizability change according to the vibration.

So, induced dipole is;

$$\mu = (\alpha_0 + \beta \sin 2\pi \nu_{vib} t) E_0 \sin 2\pi\nu t \tag{2.17}$$

applying trigonometric expansion to this formula, we get;

$$\mu = \alpha_0 E_0 sin2\pi\nu t + 1/2\beta E_0\{cos2\pi(\nu - \nu_{vib})t - cos2\pi(\nu + \nu_{vib})t \tag{2.18}$$

hence, oscillating dipole will have the $\nu - \nu_{vib}$, and $\nu + \nu_{vib}$ frequency elements.

As it seen above, if the polarizability of the molecule is not changing with the vibration, there will be no Raman scattering, since β will be equal to 0, and the dipole oscillates at the same frequency with the incident radiation.

2.2.2.1 Raman Spectrometers

Although Raman and infrared spectroscopy have complemantary properties with each other, sometimes Raman spectroscopy has advantages over infrared, sometimes infrared spectroscopy has advantages over Raman, vice versa.

For instance, one advantage in which Raman spectrometer has; simple spectra's being easily observed due to the lack of combination and overtone bands. Because, these bands seen weaker in Raman when compared with infrared spectrometer. Or for solution spectra Raman spectra has variety of alternatives.

On the other hand, one of the most important disadvantages of Raman spectroscopy is giving fluorescense of samples. Besides, absorption of monochromatic light from laser results in burning solid samples or heating the liquid samples. And if the solid samples are not crystalline generally it does not give a good spectra.

Raman spectra can be taken by dispersive Raman and FT-Raman spectrometers similar to that of IR spectrometers.

Dispersive Raman Spectrometers also contain source, monochromator, and detector as in the dispersive IR spectrometers. In Raman scattering sample is excited by sending monochromatic light from laser, then a lens focuses the scattered light on to the entrance of monochromator. Then, monochromator disperses this light to its spectrum.

The introduction of FT-Raman Spectrometers has been in the late 1980s with the development of powerful desktop computers, and with the developments in Nd:YAG lasers. Early FT-Raman spectra were obtained from near infrared FT-IR spectrometers, in which the infrared source was replaced by a sample irradiated by a Nd:YAG laser beam. Differently from dispersive Raman spectrometers, in FT-Raman spectrometers

fluorescense of samples are not observed too much, because of the using of different lasers.

2.2.3 Skeletal and Group Vibrations

If the molecules have many atoms, that is when they are more complex, their infra-red and Raman spectra will be complicated, because of molecules having 3N-6 (non-linear) or 3N-5 (linear) normal modes of vibations. Although in some atoms, normal modes of vibrations move simultaneously, the remainings move in a different way. For this reason, these normal modes of vibations are examined under two sections. Vibrations contain many atoms are named as skeletel vibrations, on the other hand vibrations that contain small groups of molecules named as characteristic group vibrations.

Skeletal vibrations occur because of the linear or chain structures with brances in molecules. Its' vibrations are generally between 1400-700 cm^{-1}. Since these vibrations give informations about the molecular structure and provide the recognition of complexes, they also called as fingerprint bands.

Group vibrations give informations about the atom groups in molecules. For instance, any molecule including CH_3 gives symmetric stretching absorption of C – H between 2850 and 2890 cm^{-1}, or gives an asymmetric stretching frequency at 2940-2980 cm^{-1} in IR spectrum. In addition to this, O-H gives absorption approximately at 3600 cm^{-1}, wheras NH_2 gives absorption at 3400 cm^{-1}. These characteristic group vibrations help in examining if the complex includes these groups or not.

In these group vibrations, if the bond lenghts of atoms are changing, it is named as stretching vibration, if the bond angles are changing, this time it is named as deformation vibration. Stretching vibrations occur in high frequencies compared with the deformation vibrations [51, 54].

CHAPTER 3

COMPUTATIONAL and EXPERIMENTAL APPROACH

3.1 Computational Details

The optimized structure and harmonic vibrational frequencies of p-tolouidine and m-tolouidine have been obtained by performing DFT-B3LYP, DFT-B3PW91 and DFT-PBEPBE calculations on our linux server cluster. The calculations were performed using Gaussian03 (with Linda) program package [55] in which the visualization of normal modes is available via Gausview program [56].

The Pople type split valence basis set of 6-311G+** (it can be also shown as 6-311G+(d,p)) and an augmented correlation consistent polarized valence quadruple-ζ (aug-cc-pVQZ) basis sets were employed in this study. The basis set aug-cc-pVQZ obtained by Dunning and co-workers is the larger one, and it has a contraction scheme of (7s,4p,3d,2f) -> [5s,4p,3d,2f] for hydrogen, and (13s,7p,4d,3f,2g) -> [6s,5p,4d,3f,2g] for carbon, oxygen, and nitrogen atoms. The smaller basis set 6-311G+** has (6s,1p) -> [4s,1p] contraction for hydrogen, and (12s,6p,1d) -> [5s,4p,1d] contraction for carbon, oxygen, and nitrogen atoms.

Polarization functions are necessary to calculate non-planar equilibrium structure of aniline and its derivatives due to the presence of the amino group's lone pair orbital.

The 6-311G+** basis set adds polarization functions in the form of five d-type functions for each atom other than H and a set of three p-type polarization functions to the hydrogen atom. This basis set has also one s-type diffuse function on hydrogen while one s-type and one p-type diffuse functions on other atoms. The correlation consistent basis set that we used (aug-cc-pVQZ) includes successively larger shells of polarization (correlating) functions (up to f-type for hydrogen, and up to g-type

functions on carbon, nitrogen, and oxygen), and it has a set diffuse functions on all atoms as well. Our molecule has a total of 1054 basis functions with aug-cc-pVQZ basis set while 239 basis functions present with 6-311G+** basis set.

3.2 Synthesis

The ligands p-tolouidine, m-tolouidine and $CuCl_2$ were purchased from Aldrich Chemical Company Inc.

The complexes Cu $[p\text{-}tol]_2$ Cl_2 and Cu $[m\text{-}tol]_2$ Cl_2 were obtained by mixing ligands (p-tolouidine and m-tolouidine) with $CuCl_2$ in the ethanol in the ratio of 2:1 respectively. After mixing these substances, samples were distilled, washed with diethylether and dried in vacuum. This process was carried out at room temperature.

3.3 Elemental Analysis

C, H, N analysis of complexes was performed in the Flash 2000 Organic Elemental Analyzer in Microanalysis labarotary in Fatih University. In order to weigh samples Precisa XR 205 SM-DR scale was used. On the other hand, Cu analysis of complexes was performed by using atomic absorption spectroscopy, which is a technique for determining the concentration of a particular metal element in a sample. Atomic absorption spectroscopy results has also been taken in Fatih University.

3.4 FT-IR Spectroscopy

The FT-IR spectra of ligands and the complexes between the range of 3500-530 cm^{-1} have been recorded by Nicolet 6700 Fourier Transform IR (FT-IR) spectrometer (see Figure 3.1) with attenuated total reflectance (ATR) sampling technique, at room temperature.

Figure 3.1 Nicolet 6700 FT-IR Spectrometer [57]

3.5 Dispersive Raman Spectroscopy

The Dispersive-Raman spectra of samples have been recorded with Nicolet DXR Dispersive Raman spectrometer (see Figure 3.2), between the range of 3500-0 cm^{-1} at room temperature. The laser with the wavelenght of 532 nm is used.

Figure 3.2 Nicolet DXR Dispersive Raman Spectrometer [57]

CHAPTER 4

EVALUATION OF THE RESULTS

4.1 Elemental Analysis of the Complexes

Theoretical and experimental values of Cu, C, H, N elemental analysis of complexes are given in Table 4.1. Since the theoretical and the experimental values being close to each other, it can be said that the complexes were obtained as pure.

Table 4.1 Elemental analysis of the complexes as percentage

	Found (cal.) %			
Comp.	Cu	C	N	H
Cu [p-tol]$_2$ Cl$_2$ (Theoretical)	17.92 (18.22)	46.67 (48.21)	7.60 (8.03)	5.01 (5.21)
Cu [m-tol]$_2$ Cl$_2$ (Theoretical)	18.73 (18.22)	44.11 (48.21)	7.23 (8.03)	4.75 (5.21)

4.2 Vibrational Spectra of the Title Molecules

Band assignments of FT-IR and dispersive Raman spectra of ligands, p-toloudine and m-toloudine will be determined with DFT calculations by using B3LYP, B3PW91, and PBEPBE methods in 6-311G+** and aug-ccPVQZ basis sets. Then the theoretical calculations with DFT and the experimental results will be compared. Moreover, after the synthesis of complexes Cu[p-tol]$_2$Cl$_2$ and Cu[m-tol]$_2$Cl$_2$, their FT-IR and dispersive Raman spectra will be examined; shifting and new bands will be discussed.

4.2.1 Conformational Properties and Vibrational Spectra of p-tolouidine

In p-tolouidine there is a methyl and an amino group joined to a planar benzene ring at para position. These methyl and amino groups are electron donating substituents in aromatic ring systems. [7, 8, 58, 59]. Although NH_2, which is amino group, participate of its electrons with the p electrons in a ring, CH_3, referred as methyl group, is influenced by hyperconjugation with close π systems. That is electronic delocalization is provided by these mechanisms and molecular orbital approach deals with this [10, 11].

Balance between opposing forces causes pyramidalized geometry in amino group in aniline and its derivatives. These forces are the stability gained by the molecule in a result of p-π conjugation of the nitrogen lone pair with the aromatic system and the stability gained by the amine which uses sp^3 orbitals during bond formation [60]. Thus, a small displacement of the nitrogen atom out of the benzene ring occurs because of the interaction between the aromatic ring and amino group.

The optimized geometry of p-toloudine can be seen in Figure 4.1. If the optimization calculations are done without any geometric restriction, it can be said that in DFT - B3LYP method with aug- ccPVQZ basis set, energy is minimum [-326.959 a.u]. That is p-toloudine is more stable in that level compared with other levels.

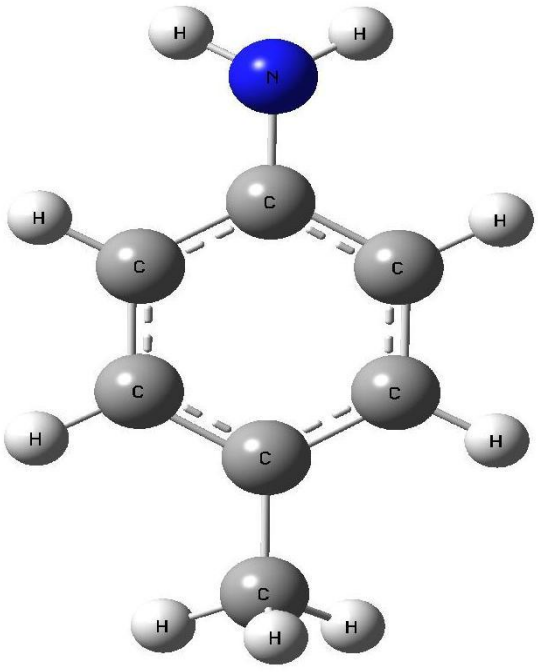

Figure 4.1 The optimized geometry of p-toloudine

Table 4.2 Total energy and geometry parameters of p-tolouidine

		DFT-B3LYP		DFT-B3PW91		DFT-PBEPBE	
	Exper.	6-311G++**	aug-ccPVQZ	6-311G++**	aug-ccPVQZ	6-311G++**	aug-ccPVQZ
Interatomic Distance (Å)							
C1-C2	1.39	1,401	1,397	1,399	1,396	1,408	1,405
C2-C3	1.40	1,391	1,387	1,389	1,385	1,397	1,394
C3-C4	1.39	1,398	1,395	1,396	1,393	1,405	1,402
C4-C5	1.40	1,398	1,394	1,396	1,392	1,405	1,402
C5-C6	1.39	1,391	1,388	1,389	1,385	1,397	1,393
C6-C1	1.36	1,401	1,397	1,399	1,396	1,408	1,405
C-N	1.43	1,401	1,397	1,395	1,392	1,402	1,399
C-CH3	1.55	1,510	1,507	1,505	1,502	1,510	1,507
N-H	1.02	1,010	1,006	1,009	1,006	1,017	1,015
C-H (ring)b	1.08	1,086	1,083	1,087	1,084	1,094	1,092
C-H (methyl)b	1.09	1,094	1,091	1,094	1,092	1,102	1,099
C1…C4		2,841	2,833	2,838	2,831	2,855	2,848
C2…C6		2,403	2,430	2,399	2,427	2,415	2,409
C3…C5		2,387	2,380	2,383	2,376	2,398	2,392
C2…C5		2,770	2,762	2,765	2,758	2,782	2,776
C6…C3		2,770	2,762	2,765	2,758	2,782	2,775
H…H (amino)		1,671	1,668	1,671	1,668	1,684	1,680
H…H (methyl)b		1,764	1,759	1,765	1,760	1,776	1,772
Bond angle (degree)							
C6-C1-C2	120.3	118.1	118.1	118.0	118.0	118.0	118.0
C1-C2-C3	119.2	120.6	120.6	120.6	120.7	120.6	120.6
C2-C3-C4	121.5	121.7	121.7	121.8	121.8	121.8	121.8
C3-C4-C5	117.8	117.2	117.2	117.1	117.1	117.1	117.1
C4-C5-C6	120.5	121.7	121.7	121.8	121.8	121.8	121.8
C5-C6-C1	120.5	120.6	120.6	120.6	120.7	120.6	120.6
N15-C1-C2 (C6)		121.0	121.0	121.0	121.0	121.0	120.9
C11-C4-C3 (C5)		121.4	121.4	121.4	121.4	121.4	121.4
H-N-H	113.0	111.7	111.9	111.8	111.9	111.7	111.8
C-C-H (methyl)b		111.4	111.4	111.4	111.4	111.5	111.5
H-C-H (methyl)b	109.5	107.5	107.5	107.5	107.4	107.4	107.4
H-N-C1		115.3	115.4	115.2	115.3	115.1	115.1
Dihedral angle (degree)							
H7-C2-C3-C4		-179.8	-179.9	-179.8	-179.8	-179.9	-179.9
H7-C2-C1-C6		180.0	-179.9	-180.0	-179.9	-179.9	-179.8
H7-C2-C1-N15		2.685	2.667	2.637	2.601	3.040	3.047
N15-C1-C2-C3		-177.3	-177.3	-177.4	-177.4	-177.0	-177.0
C2-C1-N15-H16		-157.6	-157.8	-157.6	-157.8	-157.6	-157.5
C2-C1-N15-H17		-25.12	-24.79	-25.05	-24.77	-25.43	-25.34
C6-C1-N15-H16		25.19	24.86	25.07	24.78	25.44	25.47
C6-C1-N15-H17		157.6	157.9	157.7	157.8	157.6	157.6
C4-C5-C6-H10		179.8	179.8	179.8	179.9	179.9	179.9
C3-C4-C5-H9		-179.5	-179.5	-179.6	-180.0	-179.5	-179.4
H10-C6-C5-H9		-0.326	-0.328	-0.310	-0.293	-0.302	-0.326
Total Energy (a.u.)		-326.903	-326.959	-326.773	-326.827	-326.474	-326.528

[a] Taken from Ref. [10]
[b] Averaged value.

Experimental data and geometric parameters of p-tolouidine with DFT-B3LYP, DFT-B3PW91 and DFT-PBEPBE calculations in 6-311G+** and aug- ccPVQZ basis sets and are given in Table 4.2. Experimental data is taken from Tzeng et al, 1998, [10]. According to our calculations, it can be said that, in interatomic distances all of the three methods have similar results. Nevertheless, the results in DFT-B3LYP method with 6-311G+** basis set are more compatible with the experimental data. Also in bond angles, DFT-B3LYP method has more close results to the experimental ones and both of the basis sets, 6-311G+** and aug- ccPVQZ slightly differ from each other.

FT-IR spectrum of p-toloudine between 3500-500 cm^{-1} has been taken at room temperature as shown in Figure 4.2, and p-tloudine's dispersive Raman spectrum between 3500-0 cm^{-1} is shown in Figure 4.3.

p-tolouidine has 45 normal modes of vibrations. Vibrational types and the wave numbers of normal modes are obtained with DFT-B3LYP, DFT-B3PW91 and DFT-PBEPBE methods in 6-311G+** and aug-ccPVQZ basis sets. In Tables 4.3, 4.4 and 4.5 experimental and the theoretical wave numbers and their definitions of p-tolouidine are given. In that tables, ν is used for stretching, β is for in-plane deformation, and γ is used for out-of-plane deformation. In that study scissoring, rocking, wagging, twisting and torsion vibrations are observed.

Normal modes of p-tolouidine through the bonds of C-N and C-CH_3 is represented as symmetric (A`) or asymmetric (A``) according to plane's being perpendicular to the ring plane. Thus it can be said that normal modes of p-toloudine (3N-6) is summarized as 25A` + 20A``.

As it mentioned in Tables 4.3 - 4.5, each normal mode of p-tolouidine occur from internal coordinates. The DFT calculations show the C-C stretching, in-plane C-H deformations, the NH_2 (amino group) rocking and scissoring, and in-plane CH_3 (methyl group) vibrations. The coupling schemes of these vibrations within the modes are very close to each other with the DFT-B3LYP and DFT-PBEPBE methods and two basis sets.

Table 4.3 Experimental and DFT-B3LYP level computed vibrational frequencies of p-tolouidine

Experimental[a]		B3LYP/6-311G-**				B3LYP/aug-ccPVQZ						
IR	Raman	Unscaled	Scaled	IR Intensity	Raman Activity	Unscaled	Scaled	IR Intensity	Raman Activity			Approximate description[b,c]
3418 s		3659	3575	14.54	59.28	3655	3560	14.92	57.64	A"		νNH (asym)
3337 s		3564	3482	15.97	211.2	3560	3467	16.12	228.4	A'		νNH (sym)
3222 m	3226 w	3167	3094	0.285	307.1	3167	3085	0.290	298.8	A'	2	νCH
3095 w		3163	3090	42.07	0.107	3164	3082	38.77	0.167	A"	20b	νCH
3058 w	3055 s	3148	3076	0.951	125.7	3148	3066	1.428	117.0	A"	7b	νCH
3027	3036 s	3147	3075	30.30	3.922	3148	3066	28.23	5.863	A'	13	νCH
3010	3016 s	3093	3022	19.09	65.41	3093	3013	17.59	61.40	A"		νCH_3 (asym)
2913 m		3066	2995	23.14	94.36	3065	2985	20.95	93.71	A'		νCH_3 (asym)
2860 m	2863 m, sh	3014	2945	46.71	286.8	3015	2937	45.94	325.8	A'		νCH_3 (sym)
1623 vs		1666	1628	125.6	56.34	1664	1621	107.5	66.12	A'		βNH_2 (sciss.); νCC
	1619 m	1653	1615	5.264	12.95	1652	1609	8.519	7.109	A'	8a	νCC; βNH_2 (sciss.); [βCH]
1580 w,sh		1619	1582	3.199	1.513	1620	1578	3.019	1.064	A"	8b	νCC; βCH; βNH_2 (rock.)
1514 vs		1549	1513	107.4	0.316	1554	1514	102.1	0.323	A'	19a	νCC; βCH; βNH_2 (rock.)
		1500	1466	8.565	6.700	1502	1463	7.941	4.797	A"		βCH_3 (asym)
		1489	1455	6.924	11.50	1490	1451	5.771	9.884	A'		βCH_3 (asym)
		1457	1423	0.261	0.820	1462	1424	0.245	0.539	A"	19b	νCC; βCH; βCH_3 (asym); βNH_2 (rock.)
1445 m,sh	1381 m	1415	1382	0.030	22.77	1417	1380	0.003	18.19	A'		βCH_3 (sym)
1342 w	1324 w	1354	1323	1.316	0.235	1360	1325	0.489	1.025	A"	3	βCH; βNH_2 (rock.); βCCC
1324 m		1331	1300	5.880	3.535	1330	1295	6.536	2.880	A"	14	νCC; βNH_2 (rock.); βCH; βCH_3
1282 s,sh	1285 m	1294	1264	80.68	15.36	1297	1263	83.55	14.86	A'	20a	νCN; βCH; νCC
1269 vs	1273 m	1232	1204	0.153	18.41	1234	1202	0.058	22.04	A'	7a	νCCH_3; βCH; νCC
1178 s	1219 s	1204	1176	8.696	7.032	1207	1176	8.704	7.416	A'	9a	βCH; νCC
1123 m		1151	1125	1044	0.213	1153	1123	9.387	0.093	A"	18b	βCH; βNH_2 (rock.); νCC; [βCH_3]
1075 m	845 vs	1090	1065	2.332	2.084	1090	1062	2.005	0.745	A"		βNH_2 (rock.); νCC; βCH_3; βCH
1036 w,sh		1061	1037	8.904	3.084	1066	1038	7.473	0.851	A'		γCH_3; γCCH_3; [γCH] {γCCC}

Table 4.3 Experimental and DFT-B3LYP level computed vibrational frequencies of p-tolouidine

	1030	1006	0.282	0.305	1035	1008	0.172	0.136	A′	18a	βCCC: νCC; βCH
988 w	1000	977	0.032	0.633	1002	976	0.028	0.227	A″		βCH$_3$; βCCH$_3$; {βCCC; βCN}
954 w	961	939	0.000	0.051	978	953	0.003	0.006	A″	17a	γCH; γCCC
	939	917	0.222	0.088	952	927	0.454	0.040	A′	5	γCH; {γCCC}; γCH$_3$
	850	830	2.150	43.82	853	831	3.509	48.68	A′	12	β(γ)CCC: νCC; νCN; νCCH$_3$; β(γ)CH
830 w,sh	824	805	62.71	1.299	835	813	54.45	1.995	A′	17b	γCH; γCCC; γCN; [γCH$_3$]
814 vs	820	801	0.144	0.531	830	808	0.084	0.722	A″	10a	γCH; γCCC
758 m, sh	750	733	0.496	0.818	752	732	0.669	0.646	A′	1	β(γ)CCC: νCC; νCN; νCCH$_3$; β(γ)CH
719 m	718	701	1.081	0.522	727	708	1.148	0.564	A′	4	γCCC; γCH; γNH$_2$ (wag.); γCH$_3$
695 m	648 s	659	644	0.062	5.693	662	645	0.061	4.584	A″	6b	βCCC; {βCN; βCCC}
619 w,sh		592	578	273.9	6.770	583	568	240.3	13.14	A′		γNH$_2$ (wag.); γCCC
		508	496	73.44	0.646	510	497	79.60	1.294	A′	16b	γCCC; γNH$_2$ (wag.); γCH$_3$
	468 s	469	458	3.330	8.596	470	458	4.059	7.268	A′	6a	βCCC: νCC
	417 w	418	408	0.170	0.167	422	411	0.134	0.086	A″	16a	γCCC
		410	401	0.006	0.285	411	400	0.014	0.733	A″	15	βCN; βCCC; βCCH$_3$
	338 m	321	314	2.268	2.168	323	315	2.197	1.914	A′	11	γCCH$_3$; γCCC; γCN
		299	292	0.470	0.031	301	293	0.028	0.016	A″	9b	βCN; βCCH$_3$
	275 w	265	259	19.65	0.198	279	272	17.89	0.009	A″		γNH$_2$ (twist.)
	112 vs	139	136	4.306	0.135	140	136	3.989	0.155	A′	10b	γCN; γCCH$_3$
		30	29	0.441	0.722	24	23	0.348	0.442	A″		γCH$_3$ (torsion)

[a] s, strong; vs, very strong; m, medium; w, weak; vw, very weak; sh, shoulder; br, broad; blank, not observed or measured.

[b] ν, stretching; β, in-plane deformation; γ, out-of-plane deformation

Table 4.4 Experimental and DFT-B3PW91 level computed vibrational frequencies of p-tolouidine

Experimental[a]		B3PW91/6-311G**				B3PW91/aug-ccPVQZ						
IR	Raman	Unscaled	Scaled	IR Intensity	Raman Activity	Unscaled	Scaled	IR Intensity	Raman Activity	Approximate description[b-e]		
3418 s		3687	3558	16.33	57.38	3681	3578	16.35	56.23	A"		νNH (asym)
3337 s		3587	3461	40227	207.2	3581	3481	17.83	225.1	A'		νNH (sym)
3222 m	3226 w	3178	3067	0.437	304.2	3175	3086	0.442	301.0	A'	2	νCH
3095 w		3175	3064	38.12	0.111	3172	3083	35.91	0.091	A"	20b	νCH
3058 w	3055 s	3159	3048	0.389	125.3	3156	3068	0.207	121.6	A"	7b	νCH
3027	3036 s	3158	3047	29.09	0.917	3156	3068	28.28	0.228	A'	13	νCH
3010	3016 s	3114	3005	16.80	63.77	3110	3023	15.44	60.22	A"		νCH_3 (asym)
2913 m		3087	2979	19.72	91.97	3082	2996	17.89	91.89	A'		νCH_3 (asym)
2860 m	2863 m, sh	3026	2920	44.86	288.3	3024	2939	44.29	328.2	A'		νCH_3 (sym)
1623 vs		1679	1620	101.8	69.39	1676	1629	86.68	71.53	A'		βNH_2 (sciss.); νCC
	1619 m	1654	1596	41.88	1701	1648	1602	41.26	1823	A'	8a	νCC; βNH_2 (sciss.); [βCH]
1580 w,sh		1632	1575	3222	1226	1631	1585	3037	0.818	A"	8b	νCC; βCH; βNH_2 (rock.)
1514 vs		1555	1501	111.5	0.602	1558	1514	107.7	0.675	A'	19a	νCC; βCH; βNH_2 (rock.)
		1495	1443	8547	6056	1495	1453	7929	4177	A"		βCH_3 (asym)
		1482	1430	7441	12724	1480	1439	6237	9522	A'		βCH_3 (asym)
		1459	1408	1260	1401	1460	1419	1194	1052	A"	19b	νCC; βCH; βCH_3 (asym); βNH_2 (rock.)
1445 m,sh	1381 m	1406	1357	0.070	24.35	1406	1367	0.040	19.59	A'		βCH_3 (sym)
1342 w	1324 w	1364	1316	5808	0.638	1361	1323	4423	0.046	A"	3	βCH; βNH_2 (rock.); βCCC
1324 m		1336	1289	1427	3235	1340	1302	2734	3941	A"	14	νCC; βNH_2 (rock.); βCH; βCH_3
1282 s,sh	1285 m	1308	1262	71.08	17.12	1310	1273	73.62	17.12	A'	20a	νCN; βCH; νCC
1269 vs	1273 m	1240	1197	0.801	14.76	1242	1207	0.658	17.84	A'	7a	νCCH_3; βCH; νCC
1178 s	1219 s	1201	1159	7827	6423	1202	1168	7829	6756	A'	9a	βCH; νCC
1123 m		1148	1108	10.67	0.274	1149	1117	9464	0.138	A"	18b	βCH; βNH_2 (rock.); νCC; $[\beta CH_3]$
1075 m	845 vs	1090	1052	2642	2056	1088	1058	2270	0.744	A"		βNH_2 (rock.); νCC; βCH_3; βCH
1036 w,sh		1054	1017	9639	2808	1058	1028	8108	0.804	A'		γCH_3; γCCH_3; [γCH] {γCCC}

Table 4.4 Experimental and DFT-B3PW91 level computed vibrational frequencies of p-tolouidine

	1028	992	0.421	0.335	1032	1003	0.242	0.154	A'	18a	βCCC: νCC; βCH
988 w	996	961	0.063	0.680	997	969	0.039	0.224	A"		βCH_3; βCCH_3; {βCCC; βCN}
954 w	961	927	0.001	0.048	975	948	0.001	0.006	A"	17a	γCH; γCCC
	936	903	0.254	0.110	949	922	0.577	0.036	A'	5	γCH; {γCCC}; γCH_3
											β(γ)CCC: νCC; νCN; νCCH_3;
	856	826	1558	43.36	857	833	2144	48.80	A'	12	β(γ)CH
830 w,sh	823	794	62.58	0.921	833	810	55.31	1158	A'	17b	γCH; γCCC; γCN; [γCH_3]
814 vs	820	791	0.142	0.314	828	805	0.082	0.522	A"	10a	γCH; γCCC
											β(γ)CCC: νCC; νCN; νCCH_3;
758 m, sh	754	728	0.582	0.795	756	735	0.698	0.656	A'	1	β(γ)CH
719 m	718	693	0.981	0.453	727	707	1108	0.498	A'	4	γCCC; γCH; γNH_2 (wag.); γCH_3
695 m	656	633	0.054	5626	657	639	0.054	4497	A"	6b	βCCC; {βCN; βCCC}
619 w,sh	585	565	267.1	6363	577	561	233.8	11.98	A'		γNH_2 (wag.); γCCC
	506	488	82.04	0.675	507	493	87.98	1383	A'	16b	γCCC; γNH_2 (wag.); γCH_3
468 s	468	452	2740	8296	468	455	3346	7106	A'	6a	βCCC: νCC
417 w	416	401	0.170	0.154	420	408	0.131	0.072	A"	16a	γCCC
	406	392	0.007	0.306	407	396	0.017	0.760	A"	15	βCN; βCCC; βCCH_3
338 m	322	311	2463	2085	324	315	2358	1793	A'	11	γCCH_3; γCCC; γCN
	298	288	0.257	0.032	299	291	0.279	0.012	A"	9b	βCN; βCCH_3
275 w	272	262	19.66	0.178	285	277	17.48	0.005	A"		γNH_2 (twist.)
112 vs	139	134	4514	0.133	140	136	4.160	0.149	A'	10b	γCN; γCCH_3
	29	28	0.484	0.738	27	26	0.373	0.441	A"		γCH_3 (torsion)

[a] s, strong; vs, very strong; m, medium; w, weak; vw, very weak; sh, shoulder; br, broad; blank, not observed or measured.

[b] ν, stretching; β, in-plane deformation; γ, out-of-plane deformation

Table 4.5 Experimental and DFT-PBEPBE level computed vibrational frequencies of p-tolouidine

Experimental[a]		PBEPBE/6-311G+**				PBEPBE/aug-ccPVQZ						
IR	Raman	Unscaled	Scaled	IR Intensity	Raman Activity	Unscaled	Scaled	IR Intensity	Raman Activity			Approximate description[b,c]
3418 s		3584	3606	12.90	65.89	3574	3592	12.74	65.57	A"		νNH (asym)
3337 s		3486	3507	12.50	251.3	3476	3493	11.60	275.7	A'		νNH (sym)
3222 m	3226 w	3102	3121	0.387	334.4	3097	3112	0.411	327.8	A'	2	νCH
3095 w		3098	3117	41.61	0.076	3094	3109	38.53	0.103	A"	20b	νCH
3058 w	3055 s	3082	3100	0.746	137.5	3078	3093	0.850	131.3	A"	7b	νCH
3027	3036 s	3082	3100	31.02	3.228	3078	3093	29.36	3.632	A'	13	νCH
3010	3016 s	3042	3060	16.66	68.78	3038	3053	15.29	65.81	A"		νCH_3 (asym)
2913 m		3013	3031	19.74	103.4	3009	3024	17.81	104.5	A'		νCH_3 (asym)
2860 m	2863 m, sh	2955	2973	48.14	343.2	2952	2967	47.26	387.2	A'		νCH_3 (sym)
1623 vs		1623	1633	102.9	67.56	1619	1627	83.91	71.46	A'		βNH_2 (sciss.); νCC
	1619 m	1602	1612	30.43	1.527	1597	1605	32.78	2.111	A'	8a	νCC; βNH_2 (sciss.); [βCH]
1580 w,sh		1576	1585	2.829	0.530	1575	1583	2.593	0.266	A"	8b	νCC; βCH; βNH_2 (rock.)
1514 vs		1505	1514	105.8	2.260	1507	1515	101.1	2.433	A'	19a	νCC; βCH; βNH_2 (rock.)
		1450	1459	8.325	6.365	1449	1456	7.585	4.551	A"		βCH_3 (asym)
		1436	1445	7.342	12.91	1434	1441	6.037	11.62	A'		βCH_3 (asym)
		1415	1423	1.875	1.250	1416	1423	1.734	1.048	A"	19b	νCC; βCH; βCH_3 (asym); βNH_2 (rock.)
1445 m,sh	1381 m	1359	1367	0.171	32.75	1358	1365	0.111	27.39	A'		βCH_3 (sym)
1342 w	1324 w	1348	1356	5.495	1.700	1344	1351	5.505	1.027	A"	3	βCH; βNH_2 (rock.); βCCC
1324 m		1295	1303	0.329	2.974	1300	1307	0.473	3.752	A"	14	νCC; βNH_2 (rock.); βCH; βCH_3
1282 s,sh	1285 m	1274	1282	65.40	16.08	1274	1280	67.18	15.87	A'	20a	νCN; βCH; νCC
1269 vs	1273 m	1206	1213	1.562	17.88	1207	1213	1.350	21.16	A'	7a	νCCH_3; βCH; νCC
1178 s	1219 s	1166	1173	7.415	6.970	1166	1172	7.218	7.311	A'	9a	βCH; νCC
1123 m		1118	1125	9.142	0.465	1118	1124	7.920	0.284	A"	18b	βCH; βNH_2 (rock.); νCC; $[\beta CH_3]$
1075 m	845 vs	1058	1064	3.096	2.129	1057	1062	2.841	0.822	A"		βNH_2 (rock.); νCC; βCH_3; βCH
1036 w,sh		1017	1023	10.19	3.235	1021	1026	8.466	0.999	A'		γCH_3; γCCH_3; [γCH] {γCCC}

Table 4.5 Experimental and DFT-PBEPBE level computed vibrational frequencies of p-tolouidine

	998	1004	0.308	0.272	1002	1007	0.225	0.098	A'	18a	βCCC: νCC; βCH
988 w	966	972	0.022	0.525	966	971	0.005	0.148	A"		βCH_3; βCCH_3; {βCCC; βCN}
954 w	915	920	0.001	0.072	932	937	0.002	0.016	A"	17a	γCH; γCCC
	896	901	0.089	0.061	909	914	0.290	0.046	A'	5	γCH; {γCCC}; γCH_3
	832	837	0.892	45.54	834	838	1.168	51.29	A'	12	β(γ)CCC: νCC; νCN; νCCH_3; β(γ)CH
830 w,sh	788	793	57.11	0.800	799	803	51.56	0.844	A'	17b	γCH; γCCC; γCN; [γCH_3]
814 vs	784	789	0186	0.318	792	796	0.109	0.380	A"	10a	γCH; γCCC
758 m, sh	736	740	0.387	0.486	738	742	0.392	0.397	A'	1	β(γ)CCC: νCC; νCN; νCCH_3; β(γ)CH
719 m	692	696	1.203	0.391	700	704	1.350	0.352	A'	4	γCCC; γCH; γNH_2 (wag.); γCH_3
695 m	648 s	641	0.055	5.472	638	641	0.052	4.394	A"	6b	βCCC; {βCN; βCCC}
619 w,sh	571	574	278.2	6.767	568	571	250.9	14.19	A'		γNH_2 (wag.); γCCC
	488	491	68.25	0.514	489	491	67.80	0.902	A'	16b	γCCC; γNH_2 (wag.); γCH_3
	468 s	455	458	2.994	8.449	455	457	3.397	7.194	A'	6a	βCCC: νCC
	417 w	402	404	0.152	0.280	405	407	0.120	0.159	A"	16a	γCCC
		395	397	0.037	0.358	396	398	0.060	0.908	A"	15	βCN; βCCC; βCCH_3
	338 m	310	312	1.884	2.032	311	313	1.788	1.798	A'	11	γCCH_3; γCCC; γCN
		291	293	0.009	0.060	296	297	4.565	0.025	A"	9b	βCN; βCCH_3
	275 w	276	278	18.71	0.131	285	286	12.31	0.000	A"		γNH_2 (twist.)
	112 vs	134	135	4.431	0.148	134	135	4.021	0.168	A'	10b	γCN; γCCH_3
		30	30	0.499	0.840	24	24	0.377	0.535	A"		γCH_3 (torsion)

[a] s, strong; vs, very strong; m, medium; w, weak; vw, very weak; sh, shoulder; br, broad; blank, not observed or measured.

[b] ν, stretching; β, in-plane deformation; γ, out-of-plane deformation

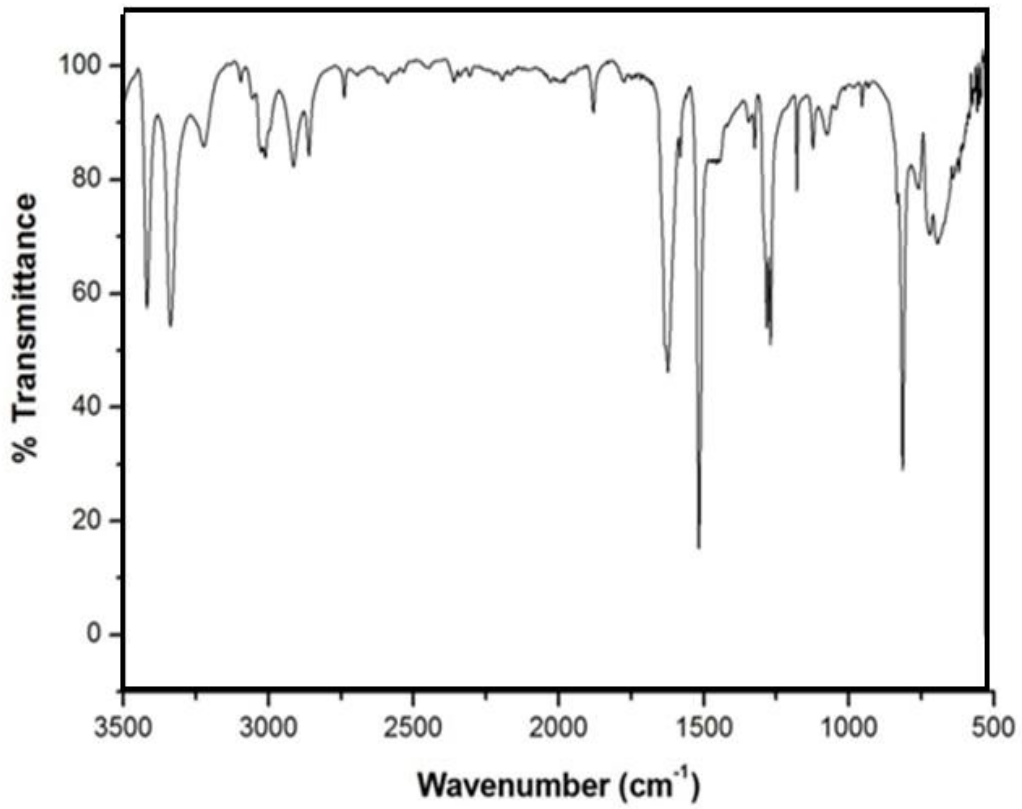

Figure 4.2 FT-IR Spectrum of p-tolouidine

FT-IR Spectrum of p-tolouidine is shown in Figure 4.2. According to DFT calculations, vibaritonal types and vibrational modes are determined. As it seen from Figure 4.2, at 3418 cm^{-1}, there is asymmetri c NH stretching motion, and at 3337 cm^{-1}, there is symetric NH stretching. CH stretching is shown between 3222 and 3095 cm^{-1}. At 1623 cm^{-1}, there is a strong peak which corresponds to NH_2 scissoring, and CC stretching vibrations. CC stretching vibrations can be seen between 1622 and 758 cm^{-1}.

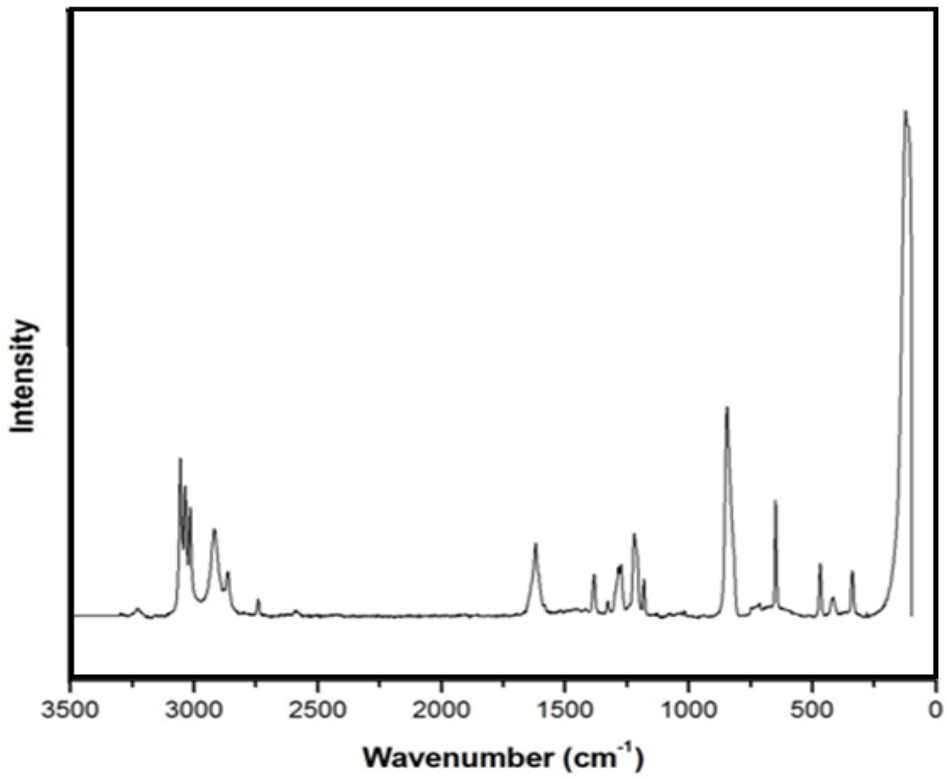

Figure 4.3 Dispersive Raman Spectrum of p-tolouidine

As seen from Figure 4.3, in dispersive Raman spectrum of p-toloudine NH asymmetric and symmetric stretching vibrations can not be determined. Between 3226 and 3036 cm^{-1}, CH stretching can be seen easily. CH_3 stretching vibrations of p-tolouidine can be seen between 3016 cm^{-1} and 2863 cm^{-1}. At 1619 cm^{-1} there is NH_2 scissoring in-plane motion. CH_3 symmetric vibration is seen at 1381 cm^{-1}, wheras CN stretching motions are observed at 1285 cm^{-1}. And CN out of plane deformation is seen at 112 cm^{-1}.

4.2.2 Conformational Properties and Vibrational Spectra of m-tolouidine

As in the case of p-tolouidine, in m-toloudine there is also a methyl and an amino group joined to a planar benzene ring, but in this case at meta position.

The staggered and eclipsed conformers of m-methylaniline have been fully optimized at the DFT-B3LYP, DFT-B3PW91 and DFT-PBEPBE levels of calculations by using both 6-311G+** and aug-ccPVQZ basis sets, as seen in Figure 4.4. Although the energy difference between these conformers has been found negligible in each type of calculations, if the optimization calculations are done without any geometric restriction, it can be said that in DFT - B3LYP method with aug-ccPVQZ basis set, the energy of m-tolouidine is minimum [-327.0712 a.u]. That is m-toloudine is more stable in DFT/B3LYP with aug- ccPVQZ basis set, compared with other methods.

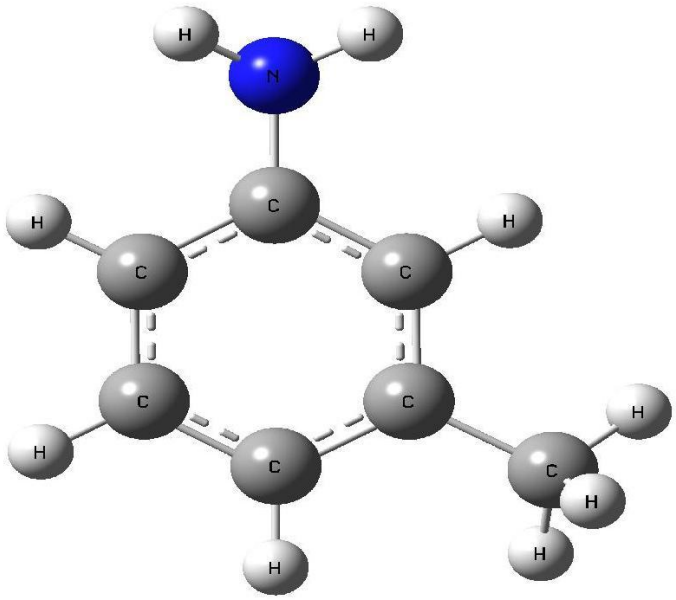

Figure 4.4 The optimized geometry of m-toloudine

Table 4.6 Total energy and geometry parameters of m-tolouidine

	DFT-B3LYP		DFT-B3PW91		DFT- PBEPBE	
	6-311G+**	aug- ccPVQZ	6-311G+**	aug- ccPVQZ	6-311G+**	aug- ccPVQZ
Interatomic Distance (Å)						
C1-C2	1.394	1.390	1.391	1.387	1.399	1.396
C2-C3	1.390	1.387	1.388	1.385	1.396	1.393
C3-C4	1.402	1.398	1.400	1.396	1.409	1.405
C4-C5	1.402	1.398	1.400	1.397	1.409	1.406
C5-C6	1.396	1.392	1.393	1.390	1.401	1.398
C6-C1	1.399	1.396	1.397	1.394	1.406	1.403
C-N	1.399	1.395	1.393	1.390	1.400	1.396
C-CH$_3$	1.510	1.507	1.505	1.502	1.510	1.507
N-H	1.009	1.006	1.008	1.006	1.017	1.014
C-H(ring)[b]	1.085	1.082	1.086	1.084	1.094	1.092
C-H(methyl)[b]	1.094	1.090	1.094	1.091	1.102	1.099
C1...C4	2.806	2.798	2.803	2.796	2.820	2.813
C2...C6	2.418	2.411	2.413	2.407	2.429	2.423
C3...C5	2.413	2.406	2.409	2.403	2.424	2.418
C2...C5	2.770	2.762	2.765	2.758	2.782	2.775
C6...C3	2.807	2.799	2.802	2.795	2.819	2.812
H..H(amino)	1.674	1.671	1.674	1.671	1.686	1.684
H..H(methyl)[b]	1.765	1.766	1.766	1.762	1.777	1.773
Angle (Degree)						
C6-C1-C2	119.9	119.9	119.9	119.9	119.9	119.9
C1-C2-C3	120.9	120.9	121.0	121.0	121.0	121.0
C2-C3-C4	119.9	119.9	119.9	119.9	119.9	119.9
C3-C4-C5	118.8	118.8	118.7	118.7	118.7	118.7
C4-C5-C6	121.5	121.5	121.6	121.6	121.6	121.6
C5-C6-C1	118.9	118.9	119.0	118.9	118.9	118.9
N15-C4-C3(C5)	120.6	120.6	120.6	120.6	120.6	120.6
C11-C6-C1(C5)	120.5	120.5	120.5	120.5	120.5	120.5
H-N-H	112.1	112.2	112.1	112.3	112.0	112.1
C-C-H(methyl)[b]	111.2	111.2	111.3	111.3	111.3	111.3
H-C-H(methyl)[b]	107.6	107.6	107.6	107.6	107.6	107.6
H-N-C1	115.6	115.7	115.5	115.6	115.4	115.4
Total Energy(a.u.)	-327.0152	-327.0712	-326.8854	-326.9399	-326.5821	-326.6367

[b] Averaged value.

Geometric parameters of m-tolouidine with DFT-B3LYP, DFT-B3PW91 and DFT-PBEPBE calculations in 6-311G+** and aug- ccPVQZ basis sets are given in Table 4.6. To the best of our knowledge, since, there is no experimental data on the geometric parameters of m-tolouidine in the literature, we could not compare the DFT calculation results given in Table 4.6 with the experimental data.

m-toloudine has also 45 normal modes of vibrations, as in p-tolouidine, and these modes have been assigned according to the detailed motion of individual atoms and

molecular symmetry. Wave numbers of normal modes, and vibrational types and the are calculated with DFT-B3LYP, DFT-B3PW91 and DFT-PBEPBE methods in 6-311G+** and aug-ccPVQZ basis sets. In tables 4.7, 4.8, and 4.9 experimental and the theoretical wave numbers and their definitions of m-tolouidine are given. Again, in that table, ν is used for stretching, β is for in-plane deformation, and γ is used for out-of-plane deformation, and scissoring, rocking, wagging, twisting and torsion vibrations are observed.

As seen from Tables 4.7-4.9, several internal coordinates contribute to each normal mode of m-tolouidine. The calculations reveal the presence of significant mixing between ring C-C stretching, in-plane C-H (ring) deformation, the amino group rocking and scissoring, and in-plane methyl vibrations. The coupling schemes of these vibrations within the modes are found almost the same with the DFT-B3LYP and DFT-PBEPBE methos. However, the DFT-B3PW91 coupling pattern is slightly different than the other two methods in some modes. Furthermore, the calculations in two basis sets are almost same. Thus both basis sets can be considered as reliable.

Table 4.7 Experimental and DFT-B3LYP level computed vibrational frequencies of m-tolouidine

Experimental[a]		B3LYP/6-311G++**				B3LYP/aug-ccPVQZ						
IR	Raman	Unscaled	Scaled	IR Intensity	Raman Activity	Unscaled	Scaled	IR Intensity	Raman Activity			Approximate description[b,c]
3431 s	3441 m, sh	3664	3440	15.16	57.28	3660	3440	15.53	55.71	A"		νNH (asym)
3350 s	3372 s	3567	3353	17.14	198.3	3563	3353	17.17	211.9	A'		νNH (sym)
3216 m	3219 w	3180	3008	17.55	215.8	3181	3009	16.23	210.8	A'	2	νCH
		3165	2995	21.40	65.22	3165	2995	19.81	63.08	A"	20b	νCH
3063 m	3050 s	3154	2985	5.176	73.02	3155	2986	5.018	71.42	A"	7b	νCH
3034 m		3143	2975	20.82	80.69	3143	2975	19.38	78.56	A'	13	νCH
	3010 m, sh	3100	2937	17.16	60.26	3099	2936	15.87	56.96	A"		νCH_3 (asym)
2917 m	2917 s	3074	2914	20.31	81.50	3072	2911	18.25	79.37	A'		νCH_3 (asym)
2862 m, sh	2857 w	3020	2866	31.32	229.0	3021	2866	30.32	256.6	A'		νCH_3 (sym)
1622 vs		1662	1628	150.8	21.51	1659	1624	139.4	22.41	A'		βNH_2 (sciss.); νCC
		1646	1613	55.98	18.25	1646	1611	51.74	16.64	A'	8a	νCC; βNH_2 (sciss.); [βCH]
1536 w, sh	1553 m	1627	1594	25.18	9.146	1628	1593	40.476	8.797	A"	8b	νCC; βCH; βNH_2 (rock.)
1494 vs	1491 m	1527	1497	38.52	1.664	1533	1501	34.68	1.496	A'	19a	νCC; βCH; βNH_2 (rock.)
1470 s		1507	1478	40.416	2.559	1510	1478	40.477	1.687	A"		βCH_3 (asym)
		1491	1462	7.157	8.649	1492	1461	6.012	7.163	A'		βCH_3 (asym)
		1471	1443	2.022	4.737	1473	1442	1.112	4.524	A"	19b	νCC; βCH; βCH_3 (asym); βNH_2 (rock.)
1377 w	1377 m	1412	1386	1.138	12.00	1415	1386	0.872	9.941	A'		βCH_3 (sym)
		1348	1324	4.662	1.198	1354	1326	3.142	0.644	A"	3	βCH; βNH_2 (rock.); βCCC
1312 m, sh		1339	1315	9.450	2.118	1338	1311	47.392	2.517	A"	14	νCC; βNH_2 (rock.); βCH; βCH_3
1293 s	1294 s	1313	1290	50.66	19.Haz	1316	1289	52.60	20.72	A'	20a	νCN; βCH; νCC
		1192	1172	2.667	1.966	1195	1171	18.31	2.815	A'	7a	νCCH_3; βCH; νCC
1171 s	1168 m	1191	1171	17.34	1.958	1194	1170	2.535	1.694	A'	9a	βCH; νCC
		1131	1113	2.138	3.593	1133	1111	1.775	3.200	A"	18b	βCH; βNH_2 (rock.); νCC; [βCH_3]
1078 w		1092	1075	1.994	1.264	1092	1071	1.669	1.442	A"		βNH_2 (rock.); νCC; βCH_3; βCH
1037 w		1058	1042	7.943	1.959	1063	1043	6.910	0.662	A'		γCH_3; γCCH_3; [γCH] {γCCC}

Table 4.7 Experimental and DFT-B3LYP level computed vibrational frequencies of m-tolouidine

		1018	1003	2.604	0.939	1021	1002	3.394	0.139	A'	18a	βCCC: νCC; βCH
996 m	999 vs	1009	995	2.486	42.43	1015	996	2.239	42.80	A"		βCH_3; βCCH_3; {βCCC; βCN}
		976	962	0.043	0.115	992	973	0.076	0.183	A"	17a	γCH; γCCC
927 m	928 w	943	930	7.484	0.772	945	928	6.853	0.183	A'	5	γCH; {γCCC}; γCH_3
871 m		876	865	8.568	0.275	889	873	8.331	0.213	A'	12	β(γ)CCC: νCC; νCN; νCCH_3; β(γ)CH
853 m, sh		861	851	7.314	0.451	872	856	6.593	0.700	A'	17b	γCH; γCCC; γCN; [γCH_3]
776 vs		782	774	49.08	1.841	791	777	41.78	2.152	A"	10a	γCH; γCCC
	738 vs	746	739	0.144	18.83	749	736	0.116	21.97	A'	1	β(γ)CCC: νCC; νCN; νCCH_3; β(γ)CH
691 s		702	696	18.38	0.330	710	698	17.78	0.135	A'	4	γCCC; γCH; γNH_2 (wag.); γCH_3
		599	596	135.2	4.468	598	589	88.28	5.754	A"	6b	βCCC; {βCN; βCCC}
	544 s	558	557	61.14	45.566	558	550	42.75	13.98	A'		γNH_2 (wag.); γCCC
		539	538	115.3	0.764	535	528	155.6	0.881	A'	16b	γCCC; γNH_2 (wag.); γCH_3
	517 s	525	525	0.923	4.842	526	519	0.821	3.803	A'	6a	βCCC: νCC
		448	450	13.46	0.162	452	447	13.29	0.144	A"	16a	γCCC
		429	431	0.677	0.228	432	427	0.619	0.406	A"	15	βCN; βCCC; βCCH_3
		294	300	6.973	1.049	306	305	16.407	0.301	A'	11	γCCH_3; γCCC; γCN
	296 m	286	293	12.17	0.317	289	288	4.673	1.296	A"	9b	βCN; βCCH_3
		222	230	3.074	1.280	224	225	2.729	1.045	A"		γNH_2 (twist.)
	217 m	202	211	6.633	1.124	203	204	6.098	1.126	A'	10b	γCN; γCCH_3
		40	54	0.115	0.805	31	37	0.077	0.517	A"		γCH_3 (torsion)

[a] s, strong; vs, very strong; m, medium; w, weak; vw, very weak; sh, shoulder; br, broad; blank, not observed or measured.

[b] ν, stretching; β, in-plane deformation; γ, out-of-plane deformation

Table 4.8 Experimental and DFT-B3PW91 level computed vibrational frequencies of m-tolouidine

Experimental[a]		B3PW91/6-311G-+**				B3PW91/aug-ccPVQZ							
IR	Raman	Unscaled	Scaled	IR Intensity	Raman Activity	Unscaled	Scaled	IR Intensity	Raman Activity				Approximate description[b,c]
3431 s	3441 m, sh	3691	3441	16.88	55.43	3685	3441	16.87	54.34	A"			νNH (asym)
3350 s	3372 s	3590	3353	18.90	194.2	3584	3353	18.51	208.5	A'			νNH (sym)
3216 m	3219 w	3192	3006	15.77	213.6	3188	3006	14.88	212.7	A'	2		νCH
		3176	2992	19.84	64.31	3173	2992	18.86	63.50	A"	20b		νCH
3063 m	3050 s	3165	2983	4.647	71.10	3162	2983	4.594	70.68	A"	7b		νCH
3034 m		3154	2973	19.46	80.02	3151	2973	18.50	79.08	A'	13		νCH
	3010 m, sh	3120	2943	14.98	58.74	3117	2943	13.83	55.62	A"			νCH_3 (asym)
2917 m	2917 s	3094	2921	17.21	79.54	3090	2920	15.40	78.10	A'			νCH_3 (asym)
2862 m, sh	2857 w	3032	2867	29.63	230.6	3030	2867	28.73	259.2	A'			νCH_3 (sym)
1622 vs		1667	1629	208.6	35.82	1665	1628	185.1	34.33	A'			βNH_2 (sciss.); νCC
		1653	1616	19.66	5.145	1650	1613	28.29	6.112	A'	8a		νCC; βNH_2 (sciss.); [βCH]
1536 w, sh	1553 m	1640	1603	14.77	6.263	1639	1602	12.33	5.140	A"	8b		νCC; βCH; βNH_2 (rock.)
1494 vs	1491 m	1532	1499	40.81	1.507	1535	1502	37.83	1.488	A'	19a		νCC; βCH; βNH_2 (rock.)
1470 s		1508	1476	30.20	2.185	1509	1476	30.14	1.568	A"			βCH_3 (asym)
		1483	1452	7.764	8.512	1482	1450	6.545	6.898	A'			βCH_3 (asym)
		1468	1437	0.648	5.670	1468	1436	0.358	5.040	A"	19b		νCC; βCH; βCH_3 (asym); βNH_2 (rock.)
1377 w	1377 m	1404	1375	1.558	13.93	1404	1374	1.297	11.80	A'			βCH_3 (sym)
		1368	1341	8.188	2.128	1364	1336	7.070	1.815	A"	3		βCH; βNH_2 (rock.); βCCC
1312 m, sh		1339	1313	19.83	5.477	1344	1316	17.30	4.913	A"	14		νCC; βNH_2 (rock.); βCH; βCH_3
1293 s	1294 s	1320	1294	31.06	13.45	1323	1296	35.44	15.81	A'	20a		νCN; βCH; νCC
		1196	1175	7.230	1.572	1198	1174	9.223	2.193	A'	7a		νCCH_3; βCH; νCC
1171 s	1168 m	1188	1167	9.909	2.559	1189	1166	8.608	2.724	A'	9a		βCH; νCC
		1131	1112	2.387	3.876	1132	1110	1.905	3.467	A"	18b		βCH; βNH_2 (rock.); νCC; $[\beta CH_3]$
1078 w		1093	1075	2.225	1.391	1092	1072	1.824	1.569	A"			βNH_2 (rock.); νCC; βCH_3; βCH

Table 4.8 Experimental and DFT-B3PW91 level computed vibrational frequencies of m-tolouidine

1037 w		1052	1036	8.485	1.983	1054	1035	7.417	0.707	A'		γCH_3; γCCH_3; [γCH] {γCCC}
		1015	1000	2.898	1.385	1016	998	4.282	0.806	A'	18a	βCCC: νCC; βCH
996 m	999 vs	1009	994	2.113	39.76	1013	995	1.353	40.29	A"		βCH_3; βCCH_3; {βCCC; βCN}
		974	960	0.026	0.099	989	972	0.068	0.158	A"	17a	γCH; γCCC
927 m	928 w	948	935	6.926	0.664	949	933	6.054	0.882	A'	5	γCH; {γCCC}; γCH_3
871 m		875	865	7.854	0.203	887	873	8.201	0.168	A'	12	β(γ)CCC: νCC; νCN; νCCH_3; β(γ)CH
853 m, sh		859	850	7.434	0.324	869	855	6.482	0.586	A'	17b	γCH; γCCC; γCN; [γCH_3]
776 vs		781	774	49.68	1.448	790	778	41.60	1.874	A"	10a	γCH; γCCC
	738 vs	748	742	0.202	18.21	750	740	0.128	21.30	A'	1	β(γ)CCC: νCC; νCN; νCCH_3; β(γ)CH
691 s		702	698	18.62	0.294	710	701	18.42	0.114	A'	4	γCCC; γCH; γNH_2 (wag.); γCH_3
		596	596	116.5	3.578	596	590	80.82	4.783	A"	6b	βCCC; {βCN; βCCC}
	544 s	555	556	60.06	10.53	555	550	39.36	13.34	A'		γNH_2 (wag.); γCCC
		537	539	133.3	0.486	532	528	165.3	1.128	A'	16b	γCCC; γNH_2 (wag.); γCH_3
	517 s	522	524	1.488	4.705	523	519	1.445	3.613	A'	6a	βCCC: νCC
		446	451	14.38	0.160	450	448	13.95	0.140	A"	16a	γCCC
		427	433	0.685	0.231	428	427	0.608	0.404	A"	15	βCN; βCCC; βCCH_3
		299	309	12.97	0.620	312	315	13.76	0.166	A'	11	γCCH_3; γCCC; γCN
	296 m	286	297	6.042	0.715	287	290	3.307	1.397	A"	9b	βCN; βCCH_3
		221	234	3.292	1.193	222	227	2.938	0.962	A"		γNH_2 (twist.)
	217 m	202	216	6.838	1.134	203	209	6.219	1.127	A'	10b	γCN; γCCH_3
		41	60	0.141	0.817	32	43	0.099	0.505	A"		γCH_3 (torsion)

[a] s, strong; vs, very strong; m, medium; w, weak; vw, very weak; sh, shoulder; br, broad; blank, not observed or measured.

[b] ν, stretching; β, in-plane deformation; γ, out-of-plane deformation

Table 4.9 Experimental and DFT-PBEPBE level computed vibrational frequencies of m-tolouidine

Experimental[a]		PBEPBE/6-311G+**				PBEPBE/aug-ccPVQZ						
IR	Raman	Unscaled	Scaled	IR Intensity	Raman Activity	Unscaled	Scaled	IR Intensity	Raman Activity			Approximate description[b,c]
3431 s	3441 m, sh	3589	3443	13.38	63.86	3580	3443	13.30	63.45	A"		νNH (asym)
3350 s	3372 s	3489	3351	13.40	233.2	3480	3350	12.59	252.6	A'		νNH (sym)
3216 m	3219 w	3117	3008	17.03	234.9	3112	3008	15.90	231.6	A'	2	νCH
		3100	2993	20.05	70.34	3097	2994	18.72	68.97	A"	20b	νCH
3063 m	3050 s	3089	2983	6.142	81.28	3086	2984	5.904	80.32	A"	7b	νCH
3034 m		3077	2972	21.60	87.83	3072	2971	20.12	85.97	A'	13	νCH
	3010 m, sh	3049	2946	14.87	61.87	3044	2945	13.86	58.96	A"		νCH_3 (asym)
2917 m	2917 s	3022	2921	16.76	88.26	3017	2920	14.76	88.45	A'		νCH_3 (asym)
2862 m, sh	2857 w	2962	2866	31.10	263.8	2959	2866	30.10	293.9	A'		νCH_3 (sym)
1622 vs		1614	1624	199.7	30.82	1610	1623	180.5	31.46	A'		βNH_2 (sciss.); νCC
		1601	1612	11.77	5.492	1596	1609	15.23	5.283	A'	8a	νCC; βNH_2 (sciss.); [βCH]
1536 w, sh	1553 m	1585	1596	15.40	5.489	1583	1596	13.82	4.742	A"	8b	νCC; βCH; βNH_2 (rock.)
1494 vs	1491 m	1483	1495	37.92	2.774	1485	1498	34.54	2.789	A'	19a	νCC; βCH; βNH_2 (rock.)
1470 s		1463	1475	29.42	2.173	1463	1476	29.69	1.554	A"		βCH_3 (asym)
		1437	1450	7.705	9.220	1434	1447	6.344	7.968	A'		βCH_3 (asym)
		1424	1437	0.522	5.981	1422	1435	0.218	5.933	A"	19b	νCC; βCH; βCH_3 (asym); βNH_2 (rock.)
1377 w	1377 m	1358	1371	2.742	16.52	1357	1370	2.119	14.72	A'		βCH_3 (sym)
		1354	1368	6.153	3.608	1350	1363	5.802	3.336	A"	3	βCH; βNH_2 (rock.); βCCC
1312 m, sh		1300	1314	25.14	7.853	1303	1317	21.75	7.002	A"	14	νCC; βNH_2 (rock.); βCH; βCH_3
1293 s	1294 s	1280	1294	20.96	10.86	1284	1298	25.13	13.07	A'	20a	νCN; βCH; νCC
		1163	1179	6.103	2.949	1165	1179	7.892	3.840	A'	7a	νCCH_3; βCH; νCC
1171 s	1168 m	1154	1170	10.14	2.687	1155	1169	8.852	2.899	A'	9a	βCH; νCC
		1100	1117	2.189	4.521	1100	1114	1.726	4.050	A"	18b	βCH; βNH_2 (rock.); νCC; $[\beta CH_3]$
1078 w		1063	1080	2.452	1.445	1062	1076	2.083	1.527	A"		βNH_2 (rock.); νCC; βCH_3; βCH
1037 w		1015	1033	8.101	2.276	1018	1033	6.499	0.921	A'		γCH_3; γCCH_3; [γCH] {γCCC}

Table 4.9 Experimental and DFT-PBEPBE level computed vibrational frequencies of m-tolouidine

		985	1003	5.408	1.307	987	1002	5.582	11.93	A'	18a	βCCC: νCC; βCH
996 m	999 vs	980	998	1.123	40.42	982	997	1.744	29.76	A"		βCH_3; βCCH_3; {βCCC; βCN}
		929	948	0.020	0.120	946	961	0.038	0.128	A"	17a	γCH; γCCC
927 m	928 w	923	942	5.578	0.887	923	938	4.847	1.031	A'	5	γCH; {γCCC}; γCH_3
												β(γ)CCC: νCC; νCN; νCCH_3;
871 m		834	854	6.919	0.200	847	862	6.733	0.139	A'	12	β(γ)CH
853 m, sh		820	840	6.949	0.426	831	846	6.460	0.582	A'	17b	γCH; γCCC; γCN; [γCH_3]
776 vs		748	769	43.88	1.775	757	772	37.67	2.012	A"	10a	γCH; γCCC
												β(γ)CCC: νCC; νCN; νCCH_3;
	738 vs	728	749	0.352	18.59	730	745	0.127	21.88	A'	1	β(γ)CH
691 s		676	698	18.97	0.362	684	700	18.05	0.147	A'	4	γCCC; γCH; γNH_2 (wag.); γCH_3
		576	599	141.2	4.473	575	591	102.1	6.604	A"	6b	βCCC; {βCN; βCCC}
	544 s	540	563	49.78	10.01	540	556	37.27	13.33	A'		γNH_2 (wag.); γCCC
		523	547	117.4	0.693	520	536	144.6	0.913	A'	16b	γCCC; γNH_2 (wag.); γCH_3
	517 s	508	532	0.559	4.472	509	525	0.144	3.372	A'	6a	βCCC: νCC
		431	456	13.14	0.121	434	450	12.60	0.118	A"	16a	γCCC
		416	441	0.719	0.394	417	433	0.580	0.597	A"	15	βCN; βCCC; βCCH_3
		302	328	14.15	0.445	313	330	13.37	0.138	A'	11	γCCH_3; γCCC; γCN
	296 m	281	307	3.811	1.040	281	298	2.809	1.671	A"	9b	βCN; βCCH_3
		211	238	3.172	1.149	213	230	2.729	0.933	A"		γNH_2 (twist.)
	217 m	197	225	6.374	1.194	198	215	5.866	1.202	A'	10b	γCN; γCCH_3
		41	70	0.188	0.901	32	50	0.148	0.558	A"		γCH_3 (torsion)

[a] s, strong; vs, vary strong; m, medium; w, weak; vw, very weak; sh, shoulder; br, broad; blank, not observed or measured.

[b] ν, stretching; β, in-plane deformation; γ, out-of-plane deformation

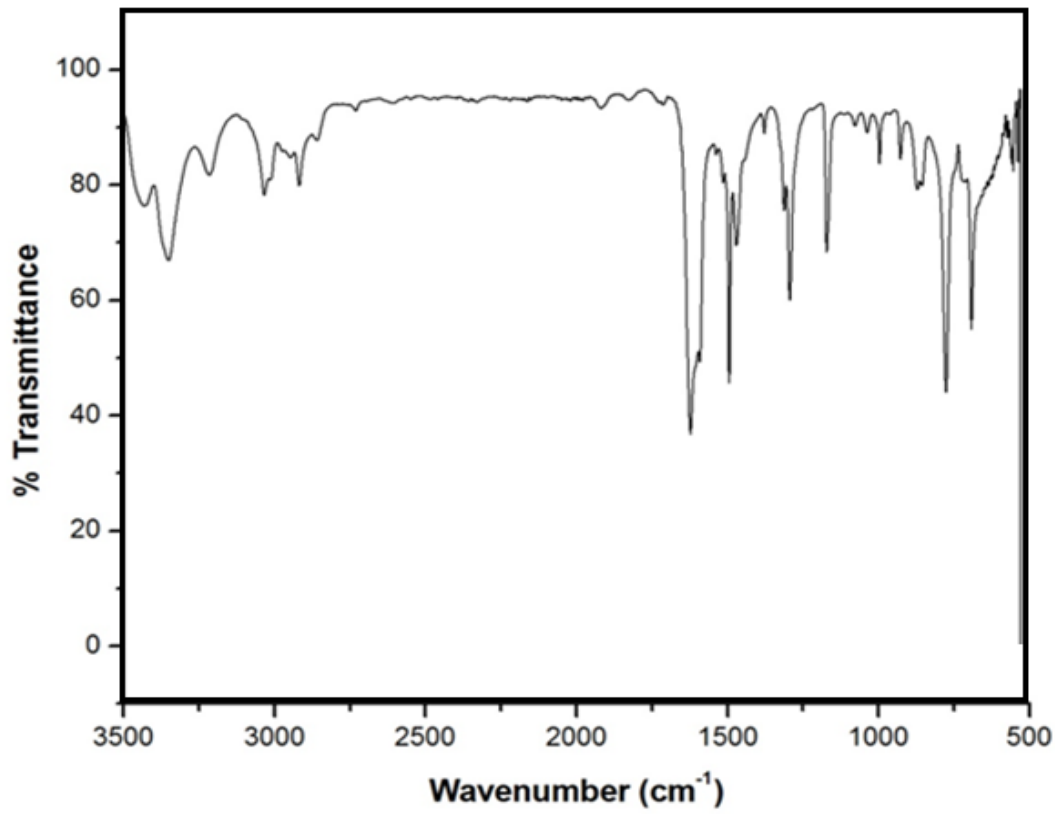

Figure 4.5 FT-IR Spectrum of m-tolouidine

In Figure 4.5 there is FT-IR Spectrum of m-tolouidine. From the figure, it can be seen at 3431 and 3350 cm^{-1}, there are NH stretching vibrations as asymmetric and symmetric respectively. Between 3216 and 3034 cm^{-1}, CH stretching vibration can bee seen. At 2917 cm^{-1}, CH_3 asymmetric vibration is seen, wheras at 2862 cm^{-1}, CH_3 symmetric vibration is seen. At 1622 cm^{-1}, NH_2 scissoring and CC stretching motions can be observed. Other CC stretching vibrations can be seen between 1622-691 cm^{-1}. CH out of plane deformations can be seen between 927 - 691 cm^{-1}. In-plane NH_2 rocking motion can be seen at1312 cm^{-1}. And out of plane NH_2 wagging motions are observed at 691 cm^{-1}.

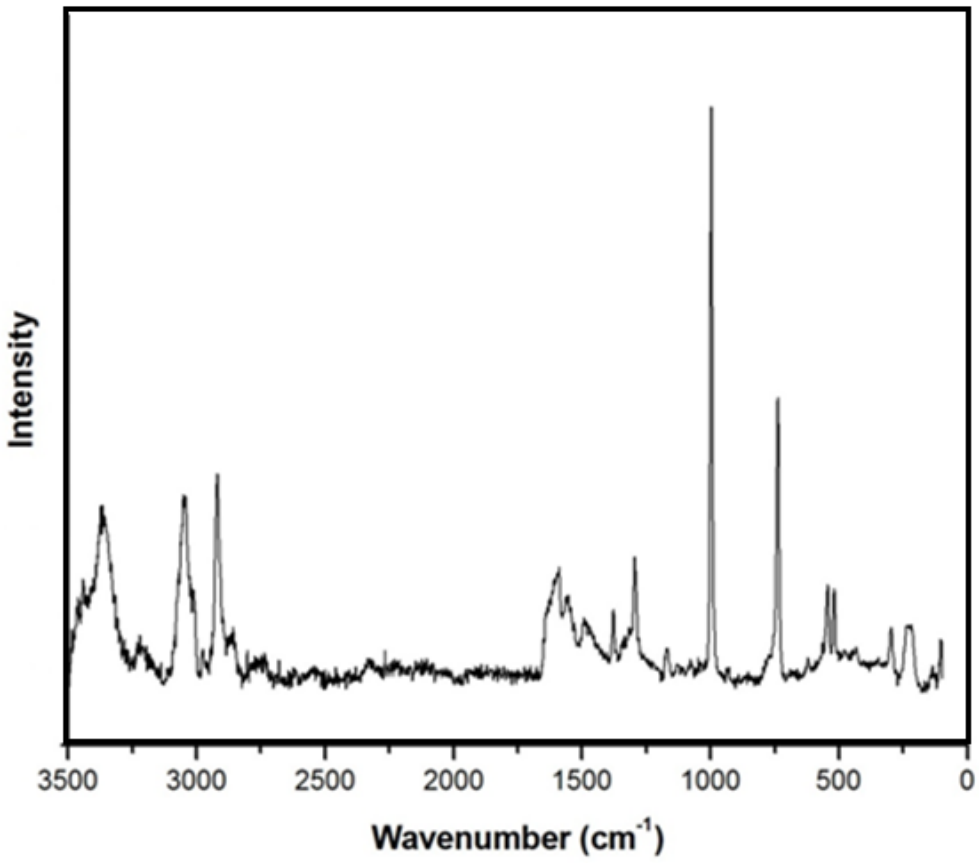

Figure 4.6 Dispersive Raman Spectrum of m-tolouidine

In Figure 4.6, dispersive Raman spectrum of m-tolouidine is shown. Since the m-tolouidine is a clourful liquid, while taking its dispersive Raman spectrum it gives some fluorescense. By decreasing the intensity and wavelenght of the laser, this spectrum is obtained. According to figure, at 3441 cm^{-1}, asymmetric NH stretching, and in 3372 cm^{-1} NH symmetric stretching vibrations are observed. Between 3219-3050 cm^{-1}, CH stretching vibrations can be seen. CH_3 stretching vibrations are shown at 3010 and 2857 cm^{-1}. At 1533 and 1491 NH_2 rocking vibrations (in-plane) are observed. CC stretching vibrations are observed between 1553-738 cm^{-1}. And at 217 cm^{-1}, out of plane CN deformation is observed.

4.2.3 Vibrational Spectra of Complexes

FT-IR and dispersive Raman spectra of $Cu[p\text{-}tol]_2Cl_2$ are given in Figure 4.9 and Figure 4.10 respectively. FT-IR and dispersive Raman spectra of $Cu[m\text{-}tol]_2Cl_2$ are also given in Figure 4.11 and Figure 4.12 respectively. The dispersive Raman spectra of copper complexes exhibit strong florescence, causing disappearance of some bands. The resolvable bands and their assignments are listed in Table 4.10. Vibrational mode assignments of free p-tolouidine and m-tolouidine are based on DFT studies.

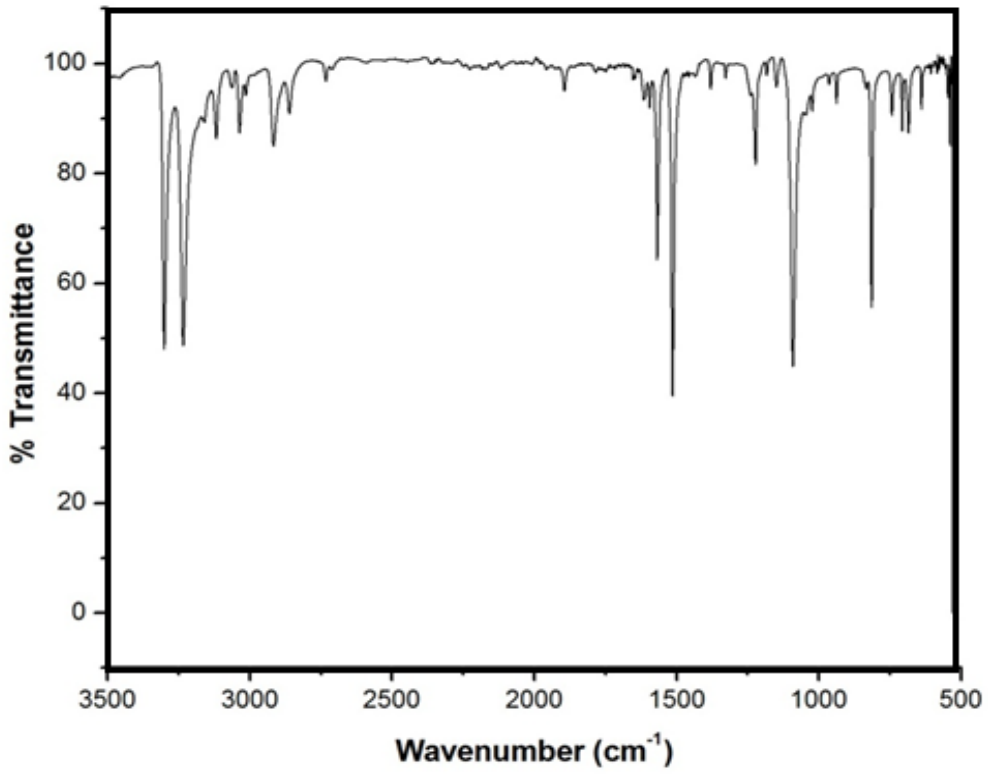

Figure 4.7 FT-IR Spectrum of Cu $[p\text{-}tol]_2\,Cl_2$

As seen from Figure 4.7, in the FT-IR Spectrum of Cu $[p\text{-}tol]_2\,Cl_2$, at 3299 cm^{-1}, NH asymmetric and at 3233 cm^{-1} NH symmetric stretching vibrations are observed. CH_3 asymmetric stretching is observed at 3008 cm^{-1}, and NH_2 scissoring is observed at 1568 cm^{-1}. In-plane CH_3 vibrations are observed in 1379 and 1327 cm^{-1}. In plane CCC vibrations are at 1023 and 937 cm^{-1}, wheras out of plane CCC vibrations are between 825-814 cm^{-1}.

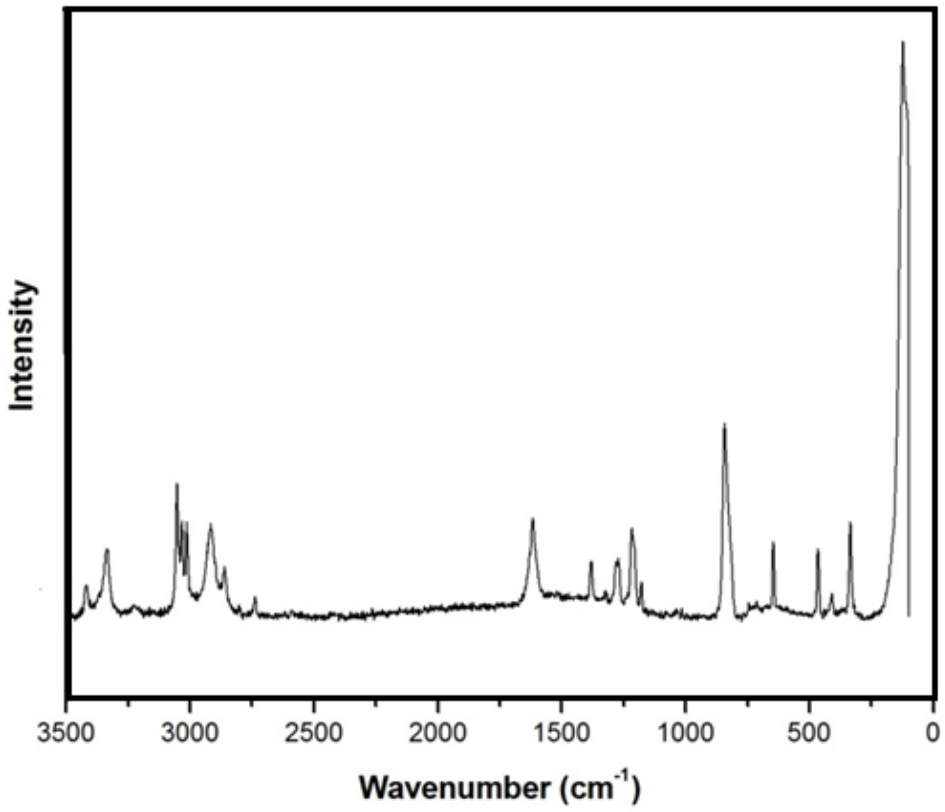

Figure 4.8 Dispersive Raman Spectrum of Cu [p-tol]$_2$ Cl_2

Dispersive Raman Spectrum of Cu [p-tol]$_2$ Cl_2 is shown in Figure 4.8. While taking dispersive Raman spectrum of the complexes, since our complexes are colourful we have encounter some difficulties such as burning of the samples. So by decreasing the intensity of the laser we have obtained these spectrums. As seen from Figure 4.8, NH asymmetric and NH symmetric vibrations can not be observed. At 3952 and 3013 cm^{-1} CH stretching vibrations are observed. In-plane CH_3 vibrations are at 1379 and 1318 cm^{-1}. And out of plane CCC vibrations are observed at 842 cm^{-1}.

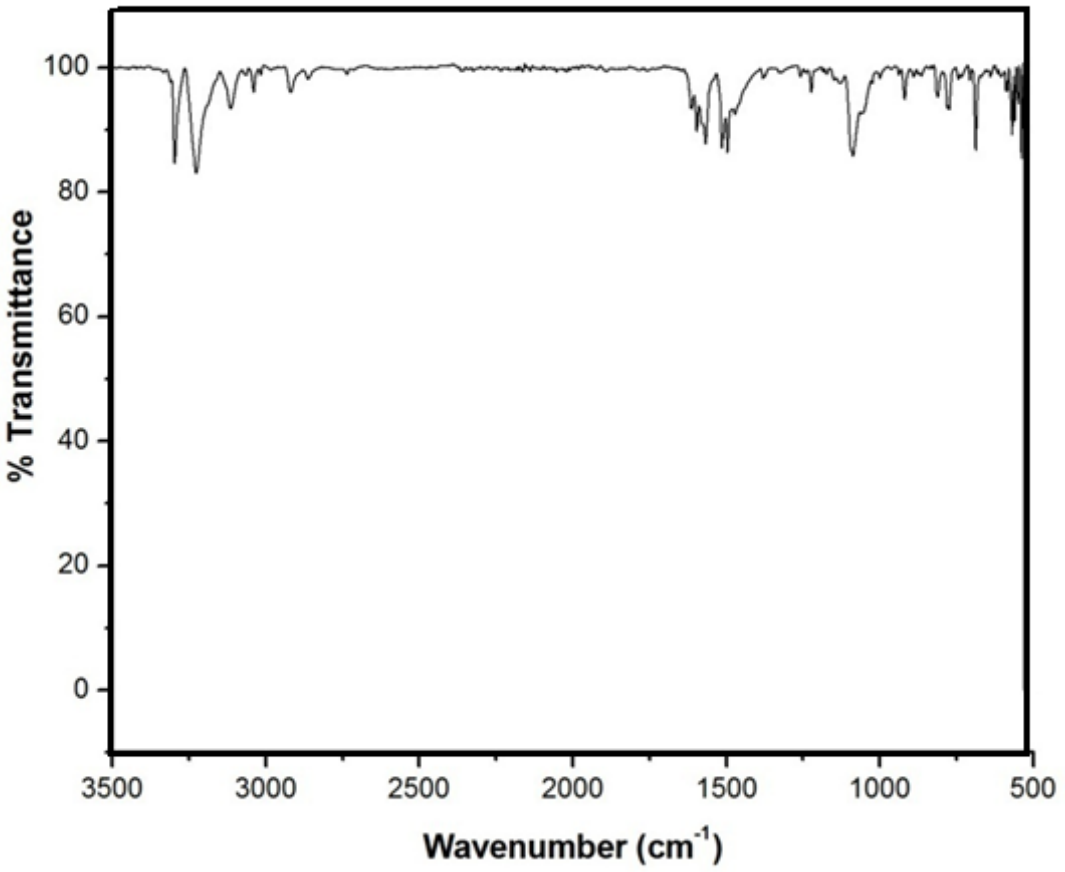

Figure 4.9 FT-IR Spectrum of Cu [m-tol]$_2$ Cl_2

FT-IR Spectrum of Cu [m-tol]$_2$ Cl_2 is obtained as Figure 4.9. According to the figure, NH asymmetric vibration is observed at 3293 cm^{-1}, wheras NH symmetric vibration is observed at 3223 cm^{-1}. At 3014 cm^{-1}, CH_3 asymmetric stretching is observed. NH_2 scissoring is observed at 1567 cm^{-1} and NH_2 rocking is observed at 1087 cm^{-1}. CC stretching vibration is observed at 1515-1471 cm^{-1}, and CN stretching vibrations are observed near 1222 cm^{-1}. In plane CCC vibrations are at 999 and 937 cm^{-1}, wheras out of plane CCC vibrations are between 918-810 cm^{-1}.

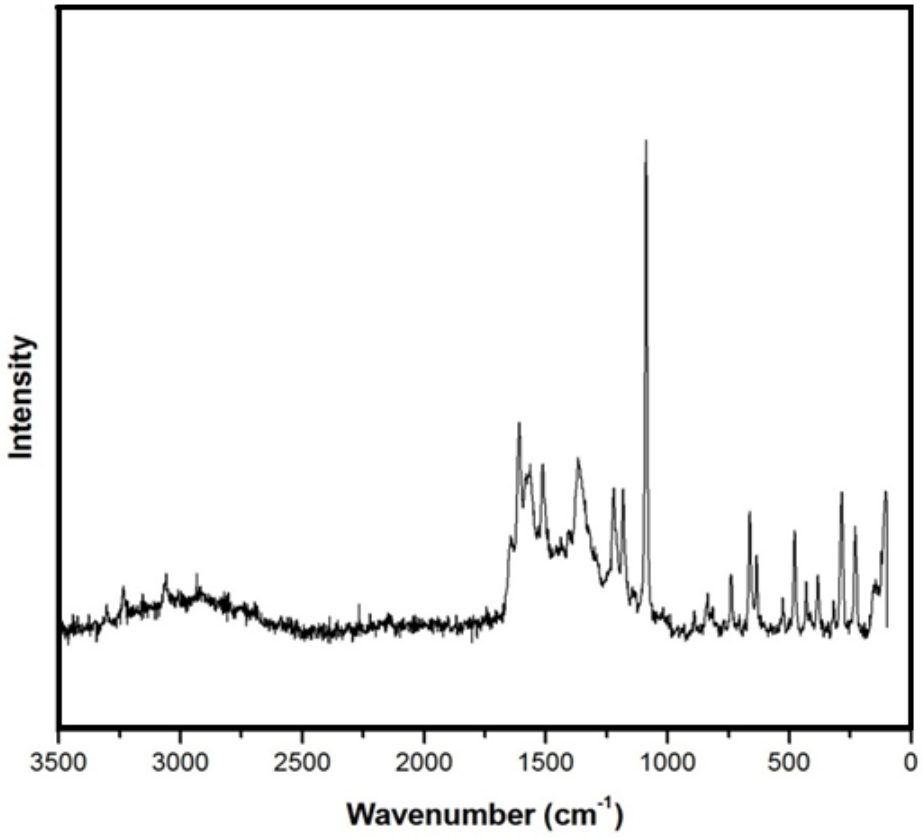

Figure 4.10 Dispersive Raman Spectrum of Cu $[m\text{-}tol]_2\,Cl_2$

As seen in Figure 4.10, the dispersive Raman spectrum of Cu $[m\text{-}tol]_2\,Cl_2$ gives strong fluorescense and because of this reason most of the bands can not be observed. According to figure, at 3228 cm^{-1} there is NH asymmetric stretching vibration. NH_2 scissoring is observed at 1564 cm^{-1} and NH_2 rocking is observed at 1088 cm^{-1}.

Table 4.10 Band Assignments of IR and Raman spectra of the complexes

p-toluidine		m-toluidine		[CuCl$_2$(p-tol)$_2$]		[CuCl$_2$(m-tol)$_2$]		
IR	Ra	IR	Ra	IR	Ra	IR	Ra	Assignment
3418 s		3431 s	3441 m, sh	3299 s		3293 vs	3228 m	νNH asym
3337 s		3350 s	3372 s	3233s		3223 vs		νNH sym
3222 m	3226 w	3216 m	3219 w	3155 m,sh				νCHring
3095 w		3063 m	3050 s	3117 m	3052 s	3114 m	3058 w	νCHring
3010	3016 s		3010 m, sh	3008 w, sh	3013 s	3014 m, sh		νCH$_3$ (asym.)
2913 m		2917 m	2917 s			2919 s		2 x 1469 over.
1623 vs		1622 vs		1568 s		1567 vs	1564 s	NH$_2$ sciss.
1580 w,sh	1619 m	1536 w, sh		1514 vs		1515 s	1512 s	νCC ring
1514 vs		1494 vs	1553 m	1430 m,sh		1471 s		νCC ring
1445 m,sh		1470 s	1491 m	1379 m	1379 m	1380 w	1368 s	βCH$_3$ (asym.)
1342 w	1381 m	1377 w	1377 m	1327 m	1318 w	1324 w		βCH$_3$ (sym.)
1324 m	1324 w	1312 m, sh			1271 m	1258 w		βCH
1282 s,sh	1285 m	1293 s	1294 s	1222 s	1217 m	1222 m	1220 s	νCN
1269 vs	1273 m			1182 w	1178 w		1182 s	νCN
1178 s	1219 s	1171 s		1148 m		1148 m	1142 w	νCCH$_3$
1123 m			1168 m	1079 vs		1087 vs	1088 vs	NH$_2$ rock.[a]
1075 m		1078 w		1041 m, sh				γCCH$_3$
1036 w,sh		1037 w		1023 m, sh		999 w		βCCC ring
988 w		996 m		937 m		937 w		βCCC ring
954 w		927 m	999 vs	825 w,sh	842 vs	918 m		γCHring; γCCC
830 w,sh	845 vs	871 m	928 w	814 vs		810 m		γCHring; γCCC
814 vs				742 m		773 s	740 m	Breathing
758 m, sh		853 m, sh		706 m				γCCC ring
719 m		776 vs	738 vs	684 s		687 vs	662 s	NH$_2$ wag.
695 m	648 s	691 s		638 w	645 s		634 s	βCCC ring
619 w,sh								βCCC ring
								ν(Cu-N)
			544 s					ν(Cu-N)
			517 s					γCCC ring
								βCNH$_2$; βCH$_3$
	468 s				467 s		478 s	NH$_2$ twist.[a]
	338 m				409 m		425 s	γCCC ring
	275 w		296 m		335 s		382 s	γCNH$_2$
			217 m		150 m, sh		144 m	ν(Cu-Cl)$_b$
	112 vs				125 vs		106 s	ν(Cu-Cl)$_b$

Keys: vs, very strong; s, strong; m, medium; w, weak; vw, very weak; b, broad; sh, shoulder; ν, stretch; β, in plane bend; γ, out of plane.

[b]Mode has not been observed, but has been found based on our DFT calculations.

All the typical bands of the p-tolouidine and m-tolouidine ligands appear in the FT-IR spectra of the metal complexes, Cu [p-tol]$_2$ Cl$_2$ and Cu [m-tol]$_2$ Cl$_2$. For instance, the NH_2 scissoring frequencies at 1623 cm^{-1} and at 1621 cm^{-1} in the p-tolouidine and m-tolouidine spectra, respectively are lowered 55 cm^{-1} by coordination. The reason for this shift is the change in nitrogen orbitals and its effect on the NH_2 force constant because of the HNH angle change [61].

Engelter et al, 1978 [62] reported an IR study of metal(II) complexes with m-tolouidine and o-tolouidine based on ^{15}N-labelling study. Although, for distinguishing NH_2 it is very useful for vibrations from phenyl ring modes, it is not sufficient for determining the assignment of the NH_2 modes. They assigned the band around 733 cm^{-1} NH_2 wagging vibration of Cu(II) complexes. However in our study we have observed the NH_2 wagging vibrations 684 cm^{-1} and 687 cm^{-1} in the spectra of [Cu(p-tol)$_2$Cl$_2$] and [Cu(m-tol)$_2$Cl$_2$] respectively. And with DFT-B3LYP calculations, the NH_2 wagging vibration has been theoretically found at 578 cm^{-1} and 555 cm^{-1} in free p-tolouidine and m-tolouidine, respectively.

The IR band at 1079 cm^{-1} (IR) in the spectra of [Cu(p-tol)$_2$Cl$_2$] and the IR and Raman bands at 1087(IR)–1088(Ra) cm^{-1} and [Cu(m-tol)$_2$Cl$_2$] have been attributed to the NH_2 rocking mode.

The νC-N stretching is seen near 1280 cm^{-1} in the substituted anilines, being relatively strong compared with the nearby bands [63]. Thus, we have assigned the bands observed at 1282 cm^{-1} and 1293 cm^{-1} as the νC-N stretching for the free p-tolouidine and m-tolouidine, respectively. Absorptions attributed to this vibration occur at lower frequencies in the complexes, in line with the decrease in the C=N double bond character [21].

In the low frequency region, especially below 500 cm^{-1} it is considered that the metal-ligand vibrations occur [20, 64]. But since we could not take the far-IR spectra of our samples, we have not observed this yet.

CHAPTER 5

CONCLUSIONS

In this study, the optimized structures of p-tolouidine and m-tolouidine, which are used as ligands have been obtained by performing Density Functional Theory (DFT) calculations on our linux server cluster. In DFT calculations B3LYP, B3PW91 and PBEPBE methods have been used. When we look at their energies, both of p-tolouidine and m-tolouidine have minimum energy in DFT-B3LYP method. That is p-tolouidine and m-tolouidine are more stable in DFT-B3LYP method.

Vibrational frequencies and the wave numbers of normal modes have also been obtained with DFT-B3LYP, DFT-B3PW91, and DFT-PBEPBE methods in 6-311G+** and aug-ccPVQZ basis sets. Calculation results have been used in the definiton of experimental infrared and Raman modes.

By using the ligands p-tolouidine and m-tolouidine, transition metal complexes, $Cu[p\text{-}tol]_2Cl_2$ and $Cu[m\text{-}tol]_2Cl_2$ are successfully synthesized. In order to determine the purity of complexes elemental (C, H, and N) analysis and with the atomic absorption spectroscopy technique Cu analyses have been performed.

Complexes have been investigated with FT-Infrared and the dispersive Raman spectroscopy techniques. In the IR and Raman spectra of the complexes characteristic ligand bands are observed. But in some ligand bands shifts are also observed. So, in the light of this mentioned fact, it can be said that $CuCl_2$ has formed bond with p-tolouidine and m-tolouidine.

REFERENCES

[1] Diaz, F.A., et al., *Synth. Met.*, 118, 25, 2001.

[2] Arjunan V., and Mohan S., *Journal of Molecular Structure,* 892, 289-299, 2008.

[3] Ng, S.C., Xu, L., *Adv. Mater,* 10,1525, 1998.

[4] Misra, R.A., et al, *Indian J. Chem.,* 38A, 141, 1999.

[5] Prevost, V., Petit, A., Pla, F., *Synth. Met.*, 104, 79, 1999.

[6] Whysner, J., et al, *Pharmacol. Ther.* 71, 107, 1996.

[7] Santos, L., et al, *Spectrochim. Acta 56A*, 1905-1915, 2000.

[8] Ballesteros, B., et al, *J. Mol. Struct.* 612, 13-28, 2002

[9] Yurdakul, S., Sen, A.I., *Vibrational Spect.* 20, 27-33, 1999.

[10] Tzeng, W.B., Narayanan, K., *J. Mol. Struct*. 446, 93-102, 1998.

[11] Tzeng, W.B., Narayanan, K., *J. Mol. Struct.* 482/483, 315-322, 1999.

[12] Akalin, E., and Akyuz, S., *J. Mol. Struct.,* 482-483, 175-181, 1999.

[13] Ikeshoji, T., and Nakanaga, T., M., *J. Electroanal. Chem.*, 528, 46, 2002.

[14] Inzelt, G., and Kertesz, V., *Electrochem. Acta*, 42, 229, 1997.

[15] Vaschetto, M. E., et al, *J. Mol. Struct.-Theochem*, 468, 209-221, 1999.

[16] Kanungo, M., et al, J. *Electroanal Chem*, 528, 46, 2002.

[17] Inzelt, G., and Kertesz, V., *Electrochim Acta*, 42, 229, 1997.

[18] DeLongchamp, D. M., Hammond, P. T., *Chem. Mater*, 16, 4799, 2004.

[19] Dong, Y., Mu, S., *Electrochim Acta,* 36, 2015, 1991.

[20] Golcuk, K., et al, *Spectrochimica Acta Part A*, 59, 1841-1847, 2003.

[21] Altun, A., et al, *Vibrational Spectroscopy*, 31, 215-225, 2003.

[22] Altun, A., et al, *Vibrational Spectroscopy*, 33 (1-2), 63-74, 2003.

[23] Golcuk, K., et al, *Journal of Molecular Structure*, 657, 385-393, 2003.

[24] Golcuk, K., et al, *Spectrochimica Acta Part A*, 60 (1-2), 303-309, 2004.

[25] Golcuk, K., et al, *Vibrational Spectroscopy*, 39 (1), 68-73, 2005.

[26] Altun, A., et al, *J. Mol. Struct.-Theochem*, 625, 17-24, 2003.

[27] Altun, A., et al, *J. Mol. Struct.-Theochem*, 637, 155-169, 2003.

[28] Kurt, M., et al., *J. Mol. Struct.-Theochem*,711, 25-32, 2004.

[29] Krishnakumar, V., and Balachandran, V., *Spectrochimica Acta Part A*, 61, 1811-1819, 2005.

[30] Krishnakumar, V., and Muthunatesan, S., *Spectrochimica Acta Part A*, 61, 199-204, 2005.

[31] Sundaraganesan, N., et al., *Spectrochimica Acta Part A*, 62, 740-751, 2005.

[32] El-Gogary, T. M., et al., *Monatshefte für Chemie*, 137, 1027-1042, 2006.

[33] Rai, A. K., et al., *Vibrational Spectroscopy*, 42, 397-402, 2006.

[34] Arjunan V., and Mohan S., *Spectrochimica Acta Part A*, 72, 436-444, 2009.

[35] Capelle, K., *Brazilian Journal of Physics*, vol. 36, no.4A, 2006.

[36] Argaman, N., and Makov, G., *Am. J. Phys.* 68 (1), 2000. Genel bilgi vs

[37] Parr, R.G., and Yang, *Density Functional Theory of Atoms and Molecules*, Oxford Univ. Press, Oxford, 1989.

[38] Koch, W., and Holthausen M. C., *A Chemist's Guide to Density Functional Theory*, Wiley-VCH Verlag GmbH, Weinheim, 2001.

[39] Dreizler, R., Gross, E., *Density Functional Theory*, Plenum Press, New York, 1995.

[40] Kohn, W., et al., *J. Phys. Chem*, 100, 12974-12980, 1996.

[41] Hohenberg, P., and Kohn, W., *Phys. Rev.*, 136, B864 – B871, 1964.

[42] Hohenberg, P., and Kohn, W., *Phys. Rev.*, 140, A1133- A1138, 1965.

[43] Becke, A.D., *J. Chem. Phys*, 98, 5648, 1993.

[44] Özen, C., *The Mechanism of Copper-Catalyzed Cyclopropanation Reaction: A DFT Study*, M.S. Thesis, Istanbul Teknik University, 2007.

[45] http://www.gaussian.com/g_tech/g_ur/k_dft.htm

[46] Jensen, F., *Introduction to Computational Chemistry*, John Wiley and Sons, England, 1999.

[47] Atkins, P., and Friedman R., *Molecular Quantum Mechanics, Oxford Univ. Press*, Fourth Edition, New York, 2005. basis setli yerler

[48] Kohanoff, J., *Electronic Structure Calculations for Solids and Molecules: Theory and Computational Methods*, Cambridge University Press, 2006.

[49] Feynman, R. P., *Six Easy Pieces*, Addison-Wesley, Reading MA, p59, 1963.

[50] Lambert, J. B., et al, *Organic Strucural Spectroscopy*, Prentice-Hall, Inc., New Jersey, 1998.

[51] Banwell C. N., and McCash, E. M., *Fundamentals of Molecular Spectroscopy*, Fourth Ed., McGraw-Hill Book Company, London, 1994.

[52] Barrow G. M., *Introduction to Molecular Spectroscopy*, McGraw-Hill Book Company, 1962.

[53]http://wpcontent.answers.com/wikipedia/commons/thumb/f/f9/Ramanscattering.svg/480px-Ramanscattering.svg.png

[54] Atkins, P. J., *Physical Chemistry*, Seventh Edition, Oxford Univ. Press, New York, 2002.

[55] Gaussian 03, Revision C.02, M. J. Frisch, G. W. Trucks, H. B. Schlegel, G. E. Scuseria, M. A. Robb, J. R. Cheeseman, J. A. Montgomery, Jr., T. Vreven, K. N. Kudin, J. C. Burant, J. M. Millam, S. S. Iyengar, J. Tomasi, V. Barone, B. Mennucci, M. Cossi, G. Scalmani, N. Rega, G. A. Petersson, H. Nakatsuji, M. Hada, M. Ehara, K. Toyota, R. Fukuda, J. Hasegawa, M. Ishida, T. Nakajima, Y. Honda, O. Kitao, H. Nakai, M. Klene, X. Li, J. E. Knox, H. P. Hratchian, J. B. Cross, V. Bakken, C. Adamo, J. Jaramillo, R. Gomperts, R. E. Stratmann, O. Yazyev, A. J. Austin, R. Cammi, C. Pomelli, J. W. Ochterski, P. Y. Ayala, K. Morokuma, G. A. Voth, P. Salvador, J. J. Dannenberg, V. G. Zakrzewski, S. Dapprich, A. D. Daniels, M. C. Strain, O. Farkas, D. K. Malick, A. D. Rabuck, K. Raghavachari, J. B. Foresman, J. V. Ortiz, Q. Cui, A. G. Baboul, S. Clifford, J. Cioslowski, B. B. Stefanov, G. Liu, A. Liashenko, P. Piskorz, I. Komaromi, R. L. Martin, D. J. Fox, T. Keith, M. A. Al-Laham, C. Y. Peng, A. Nanayakkara, M. Challacombe, P. M. W. Gill, B. Johnson, W. Chen, M. W. Wong, C. Gonzalez, and J. A. Pople, Gaussian, Inc., Wallingford CT, 2004.

[56] GaussView, Version 4.1, Roy Dennington II, Todd Keith and John Millam, Semichem, Inc., Shawnee Mission, KS, 2007.

[57] http://www.thermoscientific.com

[58] Abe, T., et al, *Chemosphere*, 45, 487-495, 2001.

[59] Palafox, M.A., et al, *J. Mol. Struct. (Theochem)*, 593, 101-131, 2002.

[60] Palafox, M.A., and Melendez, F.J., *J. Mol. Struct.(Theochem)*, 493, 171-177, 1999.

[61] Kumru, M., and Aypar, A., *Spectrochimica Acta Part A*, 47,1789, 1991

[62] C. Engelter, D. A. Thornton and M. E. Ziman. *J. Mol. Struct.*, 49, 7-15, 1978

[63] S. Akyuz, J. E. Davies, *J. Mol. Struct*., 95, 157-168, 1982.

[64] Yang, L.F., et al, *Spectrochimica Acta Part A*, 57, 2745-2764, 2001.